

# Convergence of classical optimized non-overlapping Schwarz method for Helmholtz problems in closed domains

Nicolas Marsic and Herbert De Gersem

Technische Universität Darmstadt, Institut für Teilchenbeschleunigung und Elektromagnetische Felder (TEMF)

## Abstract

In this paper we discuss the convergence of state-of-the-art optimized Schwarz transmission conditions for Helmholtz problems defined on closed domains (*i.e.* setups which do not exhibit an outgoing wave condition), as commonly encountered when modeling cavities. In particular, the impact of back-propagating waves on the Dirichlet-to-Neumann map is analyzed. Afterwards, the performance of the well-established optimized 0<sup>th</sup>-order, evanescent modes damping, optimized 2<sup>nd</sup>-order and Padé-localized square-root transmission conditions is discussed.

## 1 Introduction

It is well known that large-scale time-harmonic Helmholtz problems are hard to solve because of *i*) the pollution effect [1] and *ii*) the indefiniteness of the discretized operator [2]. While the pollution effect can be alleviated by using higher order discretization schemes [3], the indefiniteness is an intrinsic property of time-harmonic wave problems, at least with standard variational formulations [4, 5], and significantly limits the performance of classical iterative solvers, such as the generalized minimal residual method (GMRES). Of course, as an alternative to iterative algorithms, direct solvers can be used. However, because of the fill-in effect, whose minimization is known to be a NP-complete problem [6], the amount of memory needed to treat large-scale systems can become prohibitively high (see for instance [7]).

As an alternative to direct and (unpreconditioned) iterative methods for solving large-scale, high-frequency time-harmonic Helmholtz problems, domain decomposition (DD) algorithms, and optimized Schwarz (OS) techniques [8, 9, 10, 11] in particular, have attracted a lot of attention during the last decades. The key idea thereof is to: *i*) decompose the computational domain into (possibly overlapping) subdomains, creating thus new subproblems; *ii*) solve each subproblem *independently*; *iii*) exchange data at the interfaces between the subdomains via an appropriate *transmission operator* and *iv*) solve each subproblem again and iterate until convergence of the solution. Since all subproblems are solved independently, domain decomposition methods are parallel by nature<sup>1</sup> and are thus very well suited for the treatment of large-scale problems. Furthermore, as the subproblems are of reduced size, direct solvers can be used. Let also note that DD methods are rarely used as a stand-alone solver, but most of the time as a *preconditioner* for a Krylov subspace method such as GMRES. The design of such preconditioners for time-harmonic Helmholtz problems remains an active and challenging topic [13].

The convergence rate of an OS scheme strongly depends on its transmission operator. It is well known that the optimal operator is the Dirichlet-to-Neumann (DtN) map of the problem [14] (*i.e.* the operator relating the trace of the unknown field to its normal derivative at the interface between two

---

<sup>1</sup>It is also possible to solve the subproblems sequentially and to exchange data after each single solve. This family of DD methods are often referred to as sweeping algorithms, and offer some advantages, notably in terms of iteration count, which will not be further discussed in this work. More details can be found for instance in [12].

subdomains). However, the DtN map is rarely employed as it is a *non-local* operator which leads to a numerically expensive scheme. Therefore, in practice, *local approximations* of the DtN map are used, which lead to many different computational schemes [8, 9, 10, 11] (see section 5 for more details). To the best of our knowledge, all OS techniques share a common drawback: they ignore the impact of *back-propagating waves*. While this assumption is legitimate in many cases (antenna arrays [15], medical imaging reconstruction [16] or photonic waveguides [17] just to cite a few), it becomes questionable when the geometry allows resonances (even if the source does not oscillate exactly at a resonance frequency), as found for instance in lasers [18], accelerator cavities [19] or quantum electrodynamic devices [7].

The objective of this work is to determine the effect of back-propagating waves on the performance of four well-established transmission operators: the optimized 0<sup>th</sup>-order operator [8] (OO0), the evanescent modes damping operator [9] (EMDA), the optimized 2<sup>nd</sup>-order operator [10] (OO2) and the Padé-localized square-root operator [11] (PADE). This paper is organized as follows. In section 2 the Helmholtz problem as well as the optimized Schwarz scheme are presented formally on a simple cavity model problem exhibiting back-propagating waves. The optimal transmission operator of this model problem is then determined in section 3. Afterwards, in section 4, the optimal transmission condition for an unbounded problem without obstacle (*i.e.* exhibiting no back-propagating waves) is recalled and compared with the one computed in the previous section. The well-established OO0, EMDA, OO2 and PADE operators are recalled in section 5, and their performance is analyzed for a rectangular cavity problems. Section 6 shows some numerical experiments, which validate the previous theoretical analysis and extend it to circular (2D) and spherical (3D) cavities. Finally, conclusions are drawn in section 7.

## 2 Model problem and Schwarz scheme

Let  $\Omega$  be the two-dimensional domain  $[-\ell/2, +\ell/2] \times [0, h]$  depicted in Figure 1, and let  $\Gamma$  be its boundary. This domain is separated into two non-overlapping subdomains of equal size  $\Omega_0 = [-\ell/2, 0] \times [0, h]$  and  $\Omega_1 = [0, +\ell/2] \times [0, h]$ . This splitting has introduced a new artificial boundary on each subdomain: we denote by  $\Sigma_{01}$  the artificial boundary of  $\Omega_0$  and by  $\Sigma_{10}$  the artificial boundary of  $\Omega_1$ . Furthermore,  $\mathbf{n}_i$  denotes the outwardly oriented unit vector normal to  $\Sigma_{ij}$ .

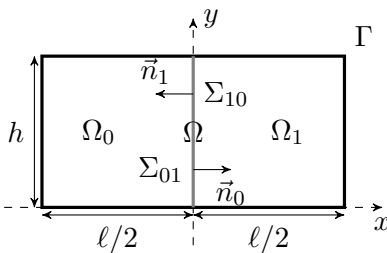


Figure 1: Domain  $\Omega$  and its decomposition into  $\Omega_1$  and  $\Omega_2$ .

Let us solve the following Helmholtz problem on  $\Omega$ :

$$\begin{cases} \operatorname{div} \mathbf{grad} p + k^2 p = g & \text{on } \Omega, \\ p = 0 & \text{on } \Gamma, \end{cases} \quad \begin{matrix} (1a) \\ (1b) \end{matrix}$$

where  $p(x, y)$  is the unknown function,  $g(x, y)$  is a known source term and  $k \in \mathbb{R}$  is the fixed wavenumber of the Helmholtz problem. Because of its boundary condition, it is obvious that (1) models a *cavity*

problem strongly exhibiting forward- and back-propagating waves. It is important to stress that for this problem to be well-defined, we must assume that  $k^2$  is not an eigenvalue of (1).

Let us now set up the following optimized non-overlapping Schwarz method, indexed by  $n$ , to solve the cavity Helmholtz problem (1):

$$\left\{ \begin{array}{ll} \operatorname{div} \mathbf{grad} p_0^{n+1} + k^2 p_0^{n+1} = g & \text{on } \Omega_0, \\ \mathbf{n}_0 \cdot \mathbf{grad} p_0^{n+1} + \mathcal{S}(p_0^{n+1}) = \mathbf{n}_0 \cdot \mathbf{grad} p_1^n + \mathcal{S}(p_1^n) & \text{on } \Sigma_{01}, \\ p_0^{n+1} = 0 & \text{on } \Gamma, \\ \\ \operatorname{div} \mathbf{grad} p_1^{n+1} + k^2 p_1^{n+1} = g & \text{on } \Omega_1, \\ \mathbf{n}_1 \cdot \mathbf{grad} p_1^{n+1} + \mathcal{S}(p_1^{n+1}) = \mathbf{n}_1 \cdot \mathbf{grad} p_0^n + \mathcal{S}(p_0^n) & \text{on } \Sigma_{10}, \\ p_1^{n+1} = 0 & \text{on } \Gamma, \end{array} \right.$$

where  $\mathcal{S}$  is the transmission operator of the optimized Schwarz algorithm and  $p_i^n(x, y)$  is the solution of the iterative procedure at iteration  $n$  and on domain  $\Omega_i$ . Once the Schwarz algorithm has converged, the solution  $p(x, y)$  of the original problem (1) is recovered by concatenating the solutions  $p_0(x, y)$  and  $p_1(x, y)$ . Since the domains do not overlap, we furthermore have that  $\mathbf{n}_0 = -\mathbf{n}_1$ . Therefore, the system of equations becomes:

$$\left\{ \begin{array}{ll} \operatorname{div} \mathbf{grad} p_0^{n+1} + k^2 p_0^{n+1} = g & \text{on } \Omega_0, & (2a) \\ +\mathbf{n}_0 \cdot \mathbf{grad} p_0^{n+1} + \mathcal{S}(p_0^{n+1}) = +\mathbf{n}_0 \cdot \mathbf{grad} p_1^n + \mathcal{S}(p_1^n) & \text{on } \Sigma_{01}, & (2b) \\ p_0^{n+1} = 0 & \text{on } \Gamma, & (2c) \\ \\ \operatorname{div} \mathbf{grad} p_1^{n+1} + k^2 p_1^{n+1} = g & \text{on } \Omega_1, & (2d) \\ -\mathbf{n}_0 \cdot \mathbf{grad} p_1^{n+1} + \mathcal{S}(p_1^{n+1}) = -\mathbf{n}_0 \cdot \mathbf{grad} p_0^n + \mathcal{S}(p_0^n) & \text{on } \Sigma_{10}, & (2e) \\ p_1^{n+1} = 0 & \text{on } \Gamma. & (2f) \end{array} \right.$$

### 3 Optimal transmission operator for the cavity problem

In order to further simplify the problem, let us now assume that the source term  $g$  is zero. Obviously, by not imposing a source in our problem the solution  $p(x, y)$  is trivially  $p = 0$  since  $k$  is not an eigenvalue. This however does not jeopardize the generality of the results derived in this section.

Let us start by taking the sine Fourier series of  $p_i^n(x, y)$  along the  $y$ -axis:

$$p_i^n(x, y) = \sum_{s \in \mathbb{S}} \widehat{p}_i^n(x, s) \sin(sy), \quad (3)$$

where the functions  $\widehat{p}_i^n(x, s)$  are the Fourier coefficients and where  $s$  is the Fourier variable, whose values are restricted to the set

$$\mathbb{S} = \left\{ s \in \mathbb{R} \mid s = m \frac{\pi}{h}, \forall m \in \mathbb{N}_0 \right\}. \quad (4)$$

Indeed, by restricting  $s$  to the set  $\mathbb{S}$ , the boundary conditions

$$\left\{ \begin{array}{ll} p_i^n(x, 0) = 0 & \forall x \in \left[ -\frac{\ell}{2}, +\frac{\ell}{2} \right], \\ p_i^n(x, h) = 0 & \forall x \in \left[ -\frac{\ell}{2}, +\frac{\ell}{2} \right], \end{array} \right.$$

are automatically satisfied. Then, by exploiting decomposition (3), the partial differential equation (2) becomes the following ordinary differential equation (ODE):

$$\left\{ \begin{array}{l} \frac{\partial^2 \widehat{p}_0^{n+1}}{\partial x^2} + (k^2 - s^2) \widehat{p}_0^{n+1} = 0 \\ \quad + \frac{\partial \widehat{p}_0^{n+1}}{\partial x} + \lambda \widehat{p}_0^{n+1} = + \frac{\partial \widehat{p}_1^n}{\partial x} + \lambda \widehat{p}_1^n \\ \quad \widehat{p}_0^{n+1} = 0 \end{array} \right. \quad \begin{array}{l} \forall x \in \left[-\frac{\ell}{2}, 0\right] \text{ and } \forall s \in \mathbb{S}, \\ \text{on } x = 0 \text{ and } \forall s \in \mathbb{S}, \\ \text{on } x = -\frac{\ell}{2} \text{ and } \forall s \in \mathbb{S}, \end{array} \quad \begin{array}{l} (5a) \\ (5b) \\ (5c) \end{array}$$

$$\left\{ \begin{array}{l} \frac{\partial^2 \widehat{p}_1^{n+1}}{\partial x^2} + (k^2 - s^2) \widehat{p}_1^{n+1} = 0 \\ \quad - \frac{\partial \widehat{p}_1^{n+1}}{\partial x} + \lambda \widehat{p}_1^{n+1} = - \frac{\partial \widehat{p}_0^n}{\partial x} + \lambda \widehat{p}_0^n \\ \quad \widehat{p}_1^{n+1} = 0 \end{array} \right. \quad \begin{array}{l} \forall x \in \left[0, +\frac{\ell}{2}\right] \text{ and } \forall s \in \mathbb{S}, \\ \text{on } x = 0 \text{ and } \forall s \in \mathbb{S}, \\ \text{on } x = +\frac{\ell}{2} \text{ and } \forall s \in \mathbb{S}, \end{array} \quad \begin{array}{l} (5d) \\ (5e) \\ (5f) \end{array}$$

where  $\lambda$  is the symbol of  $\mathcal{S}$ . Furthermore, and for simplicity, let us define  $P_i^n(s)$  as:

$$P_i^n(s) = \widehat{p}_i^n(0, s). \quad (6)$$

In order to find the best symbol  $\lambda$ , we need to determine the convergence radius of the iterative scheme (5). This objective can be achieved by:

1. deriving the fundamental solutions of (5a) and (5d);
2. fixing the integration constants with the boundary conditions (5c) and (5f) and the definition (6);
3. determining the solutions of (5a) and (5d) from the expressions found in steps 1 and 2;
4. computing  $\frac{\partial \widehat{p}_i^n(x, s)}{\partial x}$  at  $x = 0$  from the solutions  $\widehat{p}_i^n(x, s)$  found in step 3 and
5. simplifying the transmission conditions (5b) and (5e) with the expressions found in steps 3 and 4.

Let us note that this methodology is the same as the one followed in [10] for the Helmholtz problem in unbounded domains.

### 3.1 Fundamental solutions for the case $s^2 \neq k^2$

The ODEs (5a) and (5d) are nothing but a one-dimensional Helmholtz problem with wavenumber  $k^2 - s^2$ . Therefore, *by assuming  $s^2 \neq k^2$* , the fundamental solutions are:

$$\left\{ \begin{array}{l} \widehat{p}_0^{n+1}(x, s) = A_0 \exp\left[+\alpha(s)x\right] + B_0 \exp\left[-\alpha(s)x\right] \\ \widehat{p}_1^{n+1}(x, s) = A_1 \exp\left[+\alpha(s)x\right] + B_1 \exp\left[-\alpha(s)x\right] \end{array} \right. \quad \begin{array}{l} \forall x \leq 0, \forall s \in \mathbb{S}, s^2 \neq k^2, \\ \forall x \geq 0, \forall s \in \mathbb{S}, s^2 \neq k^2, \end{array} \quad \begin{array}{l} (7a) \\ (7b) \end{array}$$

where  $A_0, A_1, B_0$  and  $B_1$  are integration constants, and where

$$\alpha(s) = \begin{cases} -j\sqrt{k^2 - s^2} & \text{if } s^2 \leq k^2, \\ \sqrt{s^2 - k^2} & \text{if } s^2 \geq k^2, \end{cases} \quad \begin{array}{l} (8a) \\ (8b) \end{array}$$

with  $j$  the imaginary unit. In what follows, only the case  $s^2 \neq k^2$  is discussed. The alternative  $s^2 = k^2$  is addressed in section 3.6.

### 3.2 Integration constants for the case $s^2 \neq k^2$

Let us start by imposing the boundary conditions (6) and (5c). By inserting them into (7a), we have for all  $s \in \mathbb{S}$  and  $s^2 \neq k^2$ :

$$\left\{ \begin{array}{l} \widehat{p}_0^{n+1}(0, s) = P_0^{n+1}(s) \\ \widehat{p}_0^{n+1}\left(-\frac{\ell}{2}, s\right) = 0 \end{array} \right. \begin{array}{l} \iff \\ \iff \end{array} \begin{array}{l} A_0 + B_0 = P_0^{n+1}(s), \\ A_0 \exp\left[+\alpha(s) \frac{-\ell}{2}\right] + B_0 \exp\left[-\alpha(s) \frac{-\ell}{2}\right] = 0. \end{array}$$

Thus, it follows that:

$$\begin{cases} A_0 = P_0^{n+1}(s) - B_0, \\ B_0 = \frac{-P_0^{n+1}(s) \exp\left[+\alpha(s) \frac{-\ell}{2}\right]}{\exp\left[-\alpha(s) \frac{-\ell}{2}\right] - \exp\left[+\alpha(s) \frac{-\ell}{2}\right]}, \end{cases} \iff \begin{cases} A_0 = +P_0^{n+1}(s) \left[1 + \frac{\exp\left[-\alpha(s) \frac{\ell}{2}\right]}{\exp\left[+\alpha(s) \frac{\ell}{2}\right] - \exp\left[-\alpha(s) \frac{\ell}{2}\right]}\right], \\ B_0 = -P_0^{n+1}(s) \frac{\exp\left[-\alpha(s) \frac{\ell}{2}\right]}{\exp\left[+\alpha(s) \frac{\ell}{2}\right] - \exp\left[-\alpha(s) \frac{\ell}{2}\right]}, \end{cases}$$

and

$$\begin{cases} A_0 = +P_0^{n+1}(s) \frac{\exp\left[+\alpha(s) \frac{\ell}{2}\right]}{\exp\left[+\alpha(s) \frac{\ell}{2}\right] - \exp\left[-\alpha(s) \frac{\ell}{2}\right]}, \end{cases} \quad (9a)$$

$$\begin{cases} B_0 = -P_0^{n+1}(s) \frac{\exp\left[-\alpha(s) \frac{\ell}{2}\right]}{\exp\left[+\alpha(s) \frac{\ell}{2}\right] - \exp\left[-\alpha(s) \frac{\ell}{2}\right]}. \end{cases} \quad (9b)$$

Similarly, the integration constants of equation (7b) are found by inserting (6) and (5f) into (7b):

$$\left\{ \begin{array}{l} \widehat{p}_1^{n+1}(0, s) = P_1^{n+1}(s) \\ \widehat{p}_1^{n+1}\left(+\frac{\ell}{2}, s\right) = 0 \end{array} \right. \begin{array}{l} \iff \\ \iff \end{array} \begin{array}{l} A_1 + B_1 = P_1^{n+1}(s), \\ A_1 \exp\left[+\alpha(s) \frac{+\ell}{2}\right] + B_1 \exp\left[-\alpha(s) \frac{+\ell}{2}\right] = 0, \end{array}$$

which leads to

$$\begin{cases} A_1 = +P_1^{n+1}(s) \frac{\exp\left[-\alpha(s) \frac{\ell}{2}\right]}{\exp\left[-\alpha(s) \frac{\ell}{2}\right] - \exp\left[+\alpha(s) \frac{\ell}{2}\right]}, \end{cases} \quad (10a)$$

$$\begin{cases} B_1 = -P_1^{n+1}(s) \frac{\exp\left[+\alpha(s) \frac{\ell}{2}\right]}{\exp\left[-\alpha(s) \frac{\ell}{2}\right] - \exp\left[+\alpha(s) \frac{\ell}{2}\right]}. \end{cases} \quad (10b)$$

### 3.3 Solutions for the case $s^2 \neq k^2$

The solutions of the ODEs (5a) and (5d), subjected to the boundary conditions (6), (5c) and (5f), are then obtained by combining (7), (9) and (10):

$$\left\{ \begin{array}{l} \widehat{p}_0^{n+1}(x, s) = +P_0^{n+1}(s) \frac{\exp\left[+\alpha(s) \frac{\ell}{2}\right]}{\exp\left[+\alpha(s) \frac{\ell}{2}\right] - \exp\left[-\alpha(s) \frac{\ell}{2}\right]} \exp\left[+\alpha(s)x\right] \\ \quad - P_0^{n+1}(s) \frac{\exp\left[-\alpha(s) \frac{\ell}{2}\right]}{\exp\left[+\alpha(s) \frac{\ell}{2}\right] - \exp\left[-\alpha(s) \frac{\ell}{2}\right]} \exp\left[-\alpha(s)x\right] \quad \forall x \leq 0, \forall s \in \mathbb{S}, s^2 \neq k^2, \\ \\ \widehat{p}_1^{n+1}(x, s) = +P_1^{n+1}(s) \frac{\exp\left[-\alpha(s) \frac{\ell}{2}\right]}{\exp\left[-\alpha(s) \frac{\ell}{2}\right] - \exp\left[+\alpha(s) \frac{\ell}{2}\right]} \exp\left[+\alpha(s)x\right] \\ \quad - P_1^{n+1}(s) \frac{\exp\left[+\alpha(s) \frac{\ell}{2}\right]}{\exp\left[-\alpha(s) \frac{\ell}{2}\right] - \exp\left[+\alpha(s) \frac{\ell}{2}\right]} \exp\left[-\alpha(s)x\right] \quad \forall x \geq 0, \forall s \in \mathbb{S}, s^2 \neq k^2. \end{array} \right.$$

Furthermore, by definition of the hyperbolic sine<sup>2</sup>, we have:

$$\left\{ \begin{array}{l} \widehat{p}_0^{n+1}(x, s) = +P_0^{n+1}(s) \frac{\exp\left[+\alpha(s) \frac{\ell}{2}\right]}{2 \sinh\left[+\alpha(s) \frac{\ell}{2}\right]} \exp\left[+\alpha(s)x\right] \\ \quad - P_0^{n+1}(s) \frac{\exp\left[-\alpha(s) \frac{\ell}{2}\right]}{2 \sinh\left[+\alpha(s) \frac{\ell}{2}\right]} \exp\left[-\alpha(s)x\right] \quad \forall x \leq 0, \forall s \in \mathbb{S}, s^2 \neq k^2, \quad (11a) \\ \\ \widehat{p}_1^{n+1}(x, s) = +P_1^{n+1}(s) \frac{\exp\left[-\alpha(s) \frac{\ell}{2}\right]}{2 \sinh\left[-\alpha(s) \frac{\ell}{2}\right]} \exp\left[+\alpha(s)x\right] \\ \quad - P_1^{n+1}(s) \frac{\exp\left[+\alpha(s) \frac{\ell}{2}\right]}{2 \sinh\left[-\alpha(s) \frac{\ell}{2}\right]} \exp\left[-\alpha(s)x\right] \quad \forall x \geq 0, \forall s \in \mathbb{S}, s^2 \neq k^2. \quad (11b) \end{array} \right.$$

<sup>2</sup>We have that [20]:  $2 \sinh(x) = \exp(+x) - \exp(-x)$ .

### 3.4 Normal derivatives for the case $s^2 \neq k^2$

Thanks to the solution of equation (11), it is now possible to compute the normal derivatives of  $\widehat{p}_i^{n+1}(x, s)$ :

$$\left\{ \begin{array}{l} \frac{\partial \widehat{p}_0^{n+1}}{\partial x}(x, s) = +\alpha(s) P_0^{n+1}(s) \frac{\exp\left[+\alpha(s) \frac{\ell}{2}\right]}{2 \sinh\left[+\alpha(s) \frac{\ell}{2}\right]} \exp\left[+\alpha(s)x\right] \\ \quad + \alpha(s) P_0^{n+1}(s) \frac{\exp\left[-\alpha(s) \frac{\ell}{2}\right]}{2 \sinh\left[+\alpha(s) \frac{\ell}{2}\right]} \exp\left[-\alpha(s)x\right] \\ \frac{\partial \widehat{p}_1^{n+1}}{\partial x}(x, s) = +\alpha(s) P_1^{n+1}(s) \frac{\exp\left[-\alpha(s) \frac{\ell}{2}\right]}{2 \sinh\left[-\alpha(s) \frac{\ell}{2}\right]} \exp\left[+\alpha(s)x\right] \\ \quad + \alpha(s) P_1^{n+1}(s) \frac{\exp\left[+\alpha(s) \frac{\ell}{2}\right]}{2 \sinh\left[-\alpha(s) \frac{\ell}{2}\right]} \exp\left[-\alpha(s)x\right] \end{array} \right. \quad \forall x \leq 0, \forall s \in \mathbb{S}, s^2 \neq k^2, \quad (12a)$$

$$\forall x \geq 0, \forall s \in \mathbb{S}, s^2 \neq k^2. \quad (12b)$$

Moreover, by evaluating these derivatives at  $x = 0$ , it follows that:

$$\left\{ \begin{array}{l} \frac{\partial \widehat{p}_0^{n+1}}{\partial x}(0, s) = +\alpha(s) P_0^{n+1}(s) \frac{\exp\left[+\alpha(s) \frac{\ell}{2}\right]}{2 \sinh\left[+\alpha(s) \frac{\ell}{2}\right]} \\ \quad + \alpha(s) P_0^{n+1}(s) \frac{\exp\left[-\alpha(s) \frac{\ell}{2}\right]}{2 \sinh\left[+\alpha(s) \frac{\ell}{2}\right]} \\ \frac{\partial \widehat{p}_1^{n+1}}{\partial x}(0, s) = +\alpha(s) P_1^{n+1}(s) \frac{\exp\left[-\alpha(s) \frac{\ell}{2}\right]}{2 \sinh\left[-\alpha(s) \frac{\ell}{2}\right]} \\ \quad + \alpha(s) P_1^{n+1}(s) \frac{\exp\left[+\alpha(s) \frac{\ell}{2}\right]}{2 \sinh\left[-\alpha(s) \frac{\ell}{2}\right]} \end{array} \right. \quad \forall s \in \mathbb{S}, s^2 \neq k^2,$$

which can be further simplified into

$$\left\{ \begin{array}{l} \frac{\partial \widehat{p}_0^{n+1}}{\partial x}(0, s) = +\alpha(s) P_0^{n+1}(s) \coth\left[+\alpha(s) \frac{\ell}{2}\right] \\ \frac{\partial \widehat{p}_1^{n+1}}{\partial x}(0, s) = +\alpha(s) P_1^{n+1}(s) \coth\left[-\alpha(s) \frac{\ell}{2}\right] \end{array} \right. \quad \forall s \in \mathbb{S}, s^2 \neq k^2, \quad (13a)$$

$$\forall s \in \mathbb{S}, s^2 \neq k^2, \quad (13b)$$

by exploiting the definitions of the hyperbolic cosine and hyperbolic cotangent<sup>3</sup>.

### 3.5 Convergence radius for the case $s^2 \neq k^2$

With the normal derivative of  $\widehat{p}_i^{n+1}(x, s)$  in hand, it is now possible to simplify the transmission conditions (5b) and (5e). By combining them with (13) and (6), and by exploiting the parity of

<sup>3</sup>We have that [20]:  $2 \cosh(x) = \exp(+x) + \exp(-x)$  and  $\coth(x) = \cosh(x)/\sinh(x)$ .

$\coth(x)^4$ , we have:

$$\begin{aligned}
& \left\{ \begin{aligned} +\frac{\partial \widehat{p}_0^{n+1}}{\partial x}(0, s) + \lambda \widehat{p}_0^{n+1}(0, s) &= +\frac{\partial \widehat{p}_1^n}{\partial x}(0, s) + \lambda \widehat{p}_1^n(0, s) & \forall s \in \mathbb{S}, s^2 \neq k^2, \\ -\frac{\partial \widehat{p}_1^{n+1}}{\partial x}(0, s) + \lambda \widehat{p}_1^{n+1}(0, s) &= -\frac{\partial \widehat{p}_0^n}{\partial x}(0, s) + \lambda \widehat{p}_0^n(0, s) & \forall s \in \mathbb{S}, s^2 \neq k^2, \end{aligned} \right. \\
& \Leftrightarrow \left\{ \begin{aligned} +\alpha(s) P_0^{n+1}(s) \coth\left[+\alpha(s) \frac{\ell}{2}\right] + \lambda P_0^{n+1}(s) \\ = +\alpha(s) P_1^n(s) \coth\left[-\alpha(s) \frac{\ell}{2}\right] + \lambda P_1^n(s) & \forall s \in \mathbb{S}, s^2 \neq k^2, \\ -\alpha(s) P_1^{n+1}(s) \coth\left[-\alpha(s) \frac{\ell}{2}\right] + \lambda P_1^{n+1}(s) \\ = -\alpha(s) P_0^n(s) \coth\left[+\alpha(s) \frac{\ell}{2}\right] + \lambda P_0^n(s) & \forall s \in \mathbb{S}, s^2 \neq k^2, \end{aligned} \right. \\
& \Leftrightarrow \left\{ \begin{aligned} P_0^{n+1}(s) \left\{ \lambda + \alpha(s) \coth\left[\alpha(s) \frac{\ell}{2}\right] \right\} &= P_1^n(s) \left\{ \lambda - \alpha(s) \coth\left[\alpha(s) \frac{\ell}{2}\right] \right\} & \forall s \in \mathbb{S}, s^2 \neq k^2, \\ P_1^{n+1}(s) \left\{ \lambda + \alpha(s) \coth\left[\alpha(s) \frac{\ell}{2}\right] \right\} &= P_0^n(s) \left\{ \lambda - \alpha(s) \coth\left[\alpha(s) \frac{\ell}{2}\right] \right\} & \forall s \in \mathbb{S}, s^2 \neq k^2. \end{aligned} \right.
\end{aligned}$$

Furthermore, since the index  $n$  is arbitrary, we can further simplify the two last equations into:

$$\begin{cases} P_0^{n+1}(s) = (\rho_\lambda^{\text{close}})^2(s) P_0^{n-1}(s) & \forall s \in \mathbb{S}, s^2 \neq k^2, \\ P_1^{n+1}(s) = (\rho_\lambda^{\text{close}})^2(s) P_1^{n-1}(s) & \forall s \in \mathbb{S}, s^2 \neq k^2, \end{cases}$$

where the convergence radius  $\rho_\lambda^{\text{close}}(s)$  is given by

$$\rho_\lambda^{\text{close}}(s) = \frac{\lambda - \alpha(s) \coth\left[\alpha(s) \frac{\ell}{2}\right]}{\lambda + \alpha(s) \coth\left[\alpha(s) \frac{\ell}{2}\right]}. \quad (14)$$

From this last equation, it is then obvious that the convergence radius can be reduced to  $\rho_\lambda^{\text{close}}(s) = 0$  for all  $s^2 \neq k^2$  by selecting:

$$\lambda = \lambda_{\text{close}}^{\text{opt}}(s) = \alpha(s) \coth\left[\alpha(s) \frac{\ell}{2}\right]. \quad (15)$$

### 3.6 Case $s^2 = k^2$

Let us now treat the situation where  $s^2 = k^2$ . In this case, the ODEs (5a) and (5d) admit as fundamental solution  $\widehat{p}_i^{n+1}(x, 0) = A_i^{n+1}x + B_i^{n+1}$ . Then, by following the same approach as in section 3.2, it is found directly that  $A_0^{n+1} = P_0 2/\ell$ ,  $A_1^{n+1} = -P_0 2/\ell$ , and  $B_i^{n+1} = P_i$ . Therefore, the

<sup>4</sup>The hyperbolic cotangent is an odd function [20]:  $\coth(-x) = -\coth(x)$

normal derivatives are obviously  $\frac{\partial \widehat{p}_i^{n+1}}{\partial x}(x, 0) = A_i^{n+1}$ , leading thus to a convergence radius of the OS scheme of the form:

$$\rho_\lambda^{\text{close}}(0) = \frac{\lambda - 2/\ell}{\lambda + 2/\ell}. \quad (16)$$

This convergence radius can thus be reduced to  $\rho_\lambda^{\text{close}}(0) = 0$  by selecting

$$\lambda = \lambda_{\text{close}}^{\text{opt}}(0) = 2/\ell. \quad (17)$$

### 3.7 Optimal operator

By summarizing the results obtained in (14), (16), (15) and (17), it follows that the optimal Schwarz operator

$$\mathcal{S}_{\text{close}}^{\text{opt}} = \text{Op} \left\{ \lambda_{\text{close}}^{\text{opt}} \right\} \quad (18)$$

has as symbol:

$$\lambda_{\text{close}}^{\text{opt}}(s) = \begin{cases} \sqrt{k^2 - s^2} \cot \left[ \sqrt{k^2 - s^2} \frac{\ell}{2} \right] & \text{if } s^2 < k^2, \\ 2/\ell & \text{if } s^2 = k^2, \\ \sqrt{s^2 - k^2} \coth \left[ \sqrt{s^2 - k^2} \frac{\ell}{2} \right] & \text{if } s^2 > k^2, \end{cases} \quad (19a)$$

$$\text{if } s^2 = k^2, \quad (19b)$$

$$\text{if } s^2 > k^2, \quad (19c)$$

since  $\coth(ja) = -j \cot(a)$  and  $\cot(-a) = -\cot(a) \forall a \in \mathbb{R}$  [20]. Furthermore, the associated convergence radius is given by:

$$\rho_\lambda^{\text{close}}(s) = \frac{\lambda(s) - \lambda_{\text{close}}^{\text{opt}}(s)}{\lambda(s) + \lambda_{\text{close}}^{\text{opt}}(s)}. \quad (20)$$

From this last equation, it is clear that  $\rho_\lambda^{\text{close}}(s) = 0$  if we select  $\lambda = \lambda_{\text{close}}^{\text{opt}}$ .

## 4 Comparison between the optimal operators for cavity problems and unbounded problems without obstacles

Let us now consider the following *unbounded* Helmholtz problem without obstacles:

$$\begin{cases} \text{div } \mathbf{grad} p + k^2 p = g & \text{on } \mathbb{R}^2, \\ \lim_{r \rightarrow \infty} \sqrt{r} \left( \frac{\partial p}{\partial r} - jkp \right) = 0, \end{cases} \quad (21a)$$

$$\lim_{r \rightarrow \infty} \sqrt{r} \left( \frac{\partial p}{\partial r} - jkp \right) = 0, \quad (21b)$$

where  $r^2 = x^2 + y^2$ . In this case, it can be shown that the optimal transmission operator  $\mathcal{S}_{\text{open}}^{\text{opt}}$  for solving this problem with an OS scheme writes [11]:

$$\mathcal{S}_{\text{open}}^{\text{opt}} = \text{Op} \left( \lambda_{\text{open}}^{\text{opt}} \right) = -jk \sqrt{1 + \frac{\text{div}_\Sigma \mathbf{grad}_\Sigma}{k^2}}, \quad (22)$$

where

$$\lambda_{\text{open}}^{\text{opt}} = -jk \sqrt{1 - \frac{s^2}{k^2}}. \quad (23)$$

This non-local operator is the keystone of the construction of the OO0, EMDA, OO2 and PADE transmission operators. In particular, the four aforementioned transmission operators are nothing else but *local approximations* of  $\mathcal{S}_{\text{open}}^{\text{opt}}$ . Therefore, before studying the performance of OO0, EMDA, OO2 and PADE for solving the *cavity* problem (2), let us first compare the two optimal operators  $\mathcal{S}_{\text{open}}^{\text{opt}}$  and  $\mathcal{S}_{\text{close}}^{\text{opt}}$ , or, more precisely, their symbols. By comparing (23) and (19), it is easy to realize that

$$\lambda_{\text{close}}^{\text{opt}}(s) - \lambda_{\text{open}}^{\text{opt}}(s) = \begin{cases} \sqrt{k^2 - s^2} \cot \left[ \sqrt{k^2 - s^2} \frac{\ell}{2} \right] + j\sqrt{k^2 - s^2} & \text{if } s^2 < k^2, & (24a) \\ 2/\ell & \text{if } s^2 = k^2, & (24b) \\ \sqrt{s^2 - k^2} \coth \left[ \sqrt{s^2 - k^2} \frac{\ell}{2} \right] - \sqrt{s^2 - k^2} & \text{if } s^2 > k^2. & (24c) \end{cases}$$

Interestingly, by exploiting the definition of the hyperbolic cotangent [20], the case  $s^2 > k^2$  can be further simplified into

$$\begin{aligned} \lambda_{\text{close}}^{\text{opt}}(s) - \lambda_{\text{open}}^{\text{opt}}(s) &= \sqrt{s^2 - k^2} \coth \left[ \sqrt{s^2 - k^2} \frac{\ell}{2} \right] - \sqrt{s^2 - k^2} \\ &= \sqrt{s^2 - k^2} \left( \frac{\exp(\ell\sqrt{s^2 - k^2}) + 1}{\exp(\ell\sqrt{s^2 - k^2}) - 1} - 1 \right) \\ &= \frac{2}{\exp(\ell\sqrt{s^2 - k^2}) - 1} \sqrt{s^2 - k^2} & \text{if } s^2 > k^2, & (25) \end{aligned}$$

which yields to:

$$\lim_{s \rightarrow \infty} \lambda_{\text{close}}^{\text{opt}}(s) - \lambda_{\text{open}}^{\text{opt}}(s) = 0. \quad (26)$$

In other words, for the case  $s^2 > k^2$ , the symbol  $\lambda_{\text{open}}^{\text{opt}}(s)$  is converging towards  $\lambda_{\text{close}}^{\text{opt}}(s)$  as  $s$  grows. Furthermore, as the difference between those two symbols is decreasing exponentially,  $\lambda_{\text{open}}^{\text{opt}}(s)$  is an excellent approximation of  $\lambda_{\text{close}}^{\text{opt}}(s)$  when  $s^2 > k^2$ . For the case  $s^2 < k^2$ , as the codomains of  $\lambda_{\text{open}}^{\text{opt}}(s)$  (which is purely imaginary) and  $\lambda_{\text{close}}^{\text{opt}}(s)$  (which is purely real) do not match, the expression in (24a) cannot be further simplified. Moreover, the poles and zeros of the two symbols are very different for the case  $s^2 < k^2$ , as summarized in Table 1. For illustration purposes, the graphs of  $\lambda_{\text{open}}^{\text{opt}}$  and  $\lambda_{\text{close}}^{\text{opt}}$  are depicted in Figure 2 for different values of  $k$  ( $\Re$  and  $\Im$  are respectively denoting the real and imaginary part functions).

Criterion	$\lambda_{\text{open}}^{\text{opt}}(s)$	$\lambda_{\text{close}}^{\text{opt}}(s)$
Codomain	$j\mathbb{R}^-$ (if $s^2 \leq k^2$ ), $\mathbb{R}^+$ (if $s^2 \geq k^2$ )	$\mathbb{R}$
Zeros	one at $s = k$	many (if $s^2 < k^2$ ), none (if $s^2 > k^2$ )
Poles	none	many (if $s^2 < k^2$ ), none (if $s^2 > k^2$ )
Value at $s = 0$	0	$2/\ell$

Table 1: Comparison between  $\lambda_{\text{open}}^{\text{opt}}$  and  $\lambda_{\text{close}}^{\text{opt}}$ .

The (dis)similarities between  $\lambda_{\text{open}}^{\text{opt}}(s)$  and  $\lambda_{\text{close}}^{\text{opt}}(s)$  discussed above from a mathematical point of view can also be given a more physical interpretation. From the analysis carried out in section 3, we know that the Dirichlet-to-Neumann (DtN) map of problem (1) on  $\Sigma_{10}$  (resp.  $\Sigma_{01}$ ) is given by  $\mathcal{S}_{\text{close}}^{\text{opt}}$ . Therefore, when approximating this DtN map by  $\mathcal{S}_{\text{open}}^{\text{opt}}$ , we assume that beyond  $\Sigma_{10}$  (resp.

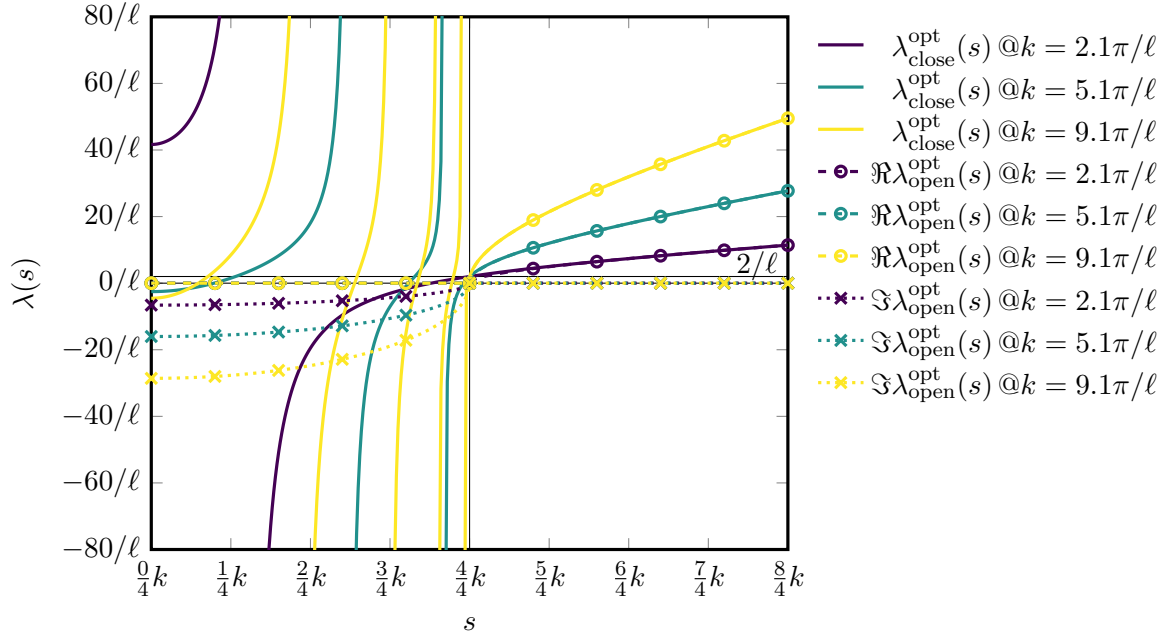


Figure 2: Graphs of  $\lambda_{\text{open}}^{\text{opt}}(s)$  and  $\lambda_{\text{close}}^{\text{opt}}(s)$  for different values of  $k$ .

$\Sigma_{01}$ ) the solution  $p(x, y)$  will behave as a wave in open space. This approximation makes sense for the component  $\hat{p}(x, s)$  such that  $s^2 > k^2$ . Indeed, in this case, the solution  $\hat{p}(x, s)$  is an *evanescent wave*, which decays as it goes away from  $x = 0$ . Therefore, it makes almost no difference whether the domain is closed or open for these components and the use of  $\mathcal{S}_{\text{open}}^{\text{opt}}$  is thus legitimate. On the other hand, the components  $\hat{p}(x, s)$  such that  $s^2 < k^2$  corresponds to waves propagating in the subdomains  $\Omega_0$  and  $\Omega_1$ . Obviously, assuming that both  $\Omega_0$  and  $\Omega_1$  correspond to unbounded domains is incorrect, meaning that  $\lambda_{\text{open}}^{\text{opt}}(s)$  cannot be used as a good approximation of  $\lambda_{\text{close}}^{\text{opt}}(s)$  in this latter case.

## 5 Behavior of transmission operators optimized for unbounded problem used in a cavity configuration

Now that we have presented and compared the optimal operators  $\mathcal{S}_{\text{close}}^{\text{opt}}$  and  $\mathcal{S}_{\text{open}}^{\text{opt}}$ , we can determine the performance of the OO0, EMDA, OO2 and PADE operators (which are nothing but approximations of  $\mathcal{S}_{\text{open}}^{\text{opt}}$ ), when used as an approximations of  $\mathcal{S}_{\text{close}}^{\text{opt}}$ . However, before starting this study, let us recall shortly the four transmission operators.

### 5.1 Recall of the OO0, EMDA, OO2 and PADE operators

#### 5.1.1 Optimized zeroth-order optimized operator (OO0)

The simplest approximate of  $\mathcal{S}_{\text{open}}^{\text{opt}}$  is simply a constant value [8], which is selected from the constant term of the Taylor expansion of  $\lambda_{\text{open}}^{\text{opt}}$ . This leads to the so-called optimized 0<sup>th</sup>-order operator (OO0), whose symbol reads:

$$\lambda_{\text{open}}^{\text{OO0}} = -jk. \quad (27)$$

### 5.1.2 Evanescent modes damping operator (EMDA)

In order to further increase the performance of the OO0 operator, a complexified wavenumber  $k_\varepsilon$  can be introduced:

$$k_\varepsilon = (1 + j\varepsilon)k, \quad (28)$$

where  $\varepsilon$  is a positive real value. This complexification leads then to the so-called evanescent modes damping operator [9] (EMDA), whose symbol reads:

$$\lambda_{\text{open}}^{\text{EMDA}} = -jk_\varepsilon. \quad (29)$$

### 5.1.3 Optimized second-order optimized operator (OO2)

By pushing the Taylor approximation strategy further, a second-order symbol can be designed:

$$\lambda_{\text{open}}^{\text{OO2}} = a + bs^2, \quad (30)$$

where  $a$  and  $b$  are two complex-valued constants, chosen to optimize the convergence rate of the Schwarz scheme [10]. Let us note that the optimal choice for  $a$  and  $b$  differs from the coefficients of the Taylor expansion. The operator associated with this symbol is classically referred to as the optimized second-order operator (OO2).

### 5.1.4 Padé-localized square-root transmission condition (PADE)

As an alternative to the Taylor expansion, a Padé decomposition of the square-root symbol (23) can be employed. This strategy leads to the following approximation with  $N_p$  Padé terms [11]:

$$\lambda_{\text{open}}^{\text{Padé}} = -jkC_0 - jk \sum_{p=1}^{N_p} \left( A_p \frac{s^2}{k_\varepsilon^2} \right) \left( 1 + B_p \frac{s^2}{k_\varepsilon^2} \right)^{-1}. \quad (31)$$

The coefficients  $C_0$ ,  $A_p$  and  $B_p$  are given by

$$C_0 = e^{j\xi/2} R_{N_p}(e^{-j\xi} - 1), \quad A_p = \frac{e^{-j\xi/2} a_p}{[1 + b_p(e^{-j\xi} - 1)]^2}, \quad B_p = \frac{e^{-j\xi} b_p}{1 + b_p(e^{-j\xi} - 1)},$$

where:

- $\xi$  is a rotation angle of the branch cut of the square-root function and is usually taken as  $\pi/4$ ;
- $R_{N_p}(z)$  is the standard real-valued Padé approximation of order  $N_p$  of  $\sqrt{1+z}$ , that is

$$R_{N_p}(z) = 1 + \sum_{p=1}^{N_p} \frac{a_p z}{1 + b_p z};$$

- $a_p$  and  $b_p$  are defined as

$$a_p = \frac{2}{2N_p + 1} \sin^2 \left( \frac{p\pi}{2N_p + 1} \right), \quad b_p = \cos^2 \left( \frac{p\pi}{2N_p + 1} \right).$$

## 5.2 Transmission operators for the open problem as an approximation of the optimal transmission operator for the closed problem

Now that the OO0, EMDA, OO2 and PADE operators are recalled, let us analyze their performance, when the symbols  $\lambda_{\text{open}}^{\text{OO0}}$ ,  $\lambda_{\text{open}}^{\text{EMDA}}$ ,  $\lambda_{\text{open}}^{\text{OO2}}$  and  $\lambda_{\text{open}}^{\text{Padé}}$  are used to approximate  $\lambda_{\text{close}}^{\text{opt}}$ . Because of the asymptotic behavior of  $\lambda_{\text{close}}^{\text{opt}}(s) - \lambda_{\text{open}}^{\text{opt}}(s)$  given in (26), we already know that OO0, EMDA, OO2 and PADE will be good approximations of  $\mathcal{S}_{\text{close}}^{\text{opt}}$  (or, at least, as good as they were for  $\mathcal{S}_{\text{open}}^{\text{opt}}$ ) for the *evanescent modes*.

### 5.2.1 Optimized zeroth-order operator (OO0)

In the case of the OO0 symbol (27), and given the convergence radius  $\rho_{\lambda}^{\text{close}}(s)$  of the Schwarz scheme (2), we have that:

$$\rho_{\lambda_{\text{open}}^{\text{OO0}}}^{\text{close}}(s) = \frac{-jk - \lambda_{\text{close}}^{\text{opt}}(s)}{-jk + \lambda_{\text{close}}^{\text{opt}}(s)}.$$

Therefore, since  $\lambda_{\text{close}}^{\text{opt}}(s)$  is real-valued, the modulus of  $\rho_{\lambda_{\text{open}}^{\text{OO0}}}^{\text{close}}(s)$  is then simply:

$$\left| \rho_{\lambda_{\text{open}}^{\text{OO0}}}^{\text{close}}(s) \right|^2 = 1 \quad \forall s \in \mathbb{S}. \quad (32)$$

This last result can be compared to the unbounded case, where the modulus of the convergence radius  $\left| \rho_{\lambda_{\text{open}}^{\text{OO0}}}^{\text{open}}(s) \right|$  is [14] (assuming no overlap):

$$\left| \rho_{\lambda_{\text{open}}^{\text{OO0}}}^{\text{open}}(s) \right| \begin{cases} < 1 \\ = 1 \end{cases} \quad \begin{cases} \text{if } s^2 < k^2, \\ \text{if } s^2 \geq k^2. \end{cases} \quad (33a)$$

$$(33b)$$

As expected, the behaviors of  $\left| \rho_{\lambda_{\text{open}}^{\text{OO0}}}^{\text{close}}(s) \right|$  and  $\left| \rho_{\lambda_{\text{open}}^{\text{OO0}}}^{\text{open}}(s) \right|$  are identical when  $s^2 > k^2$ . On the other hand, compared to the unbounded problem, the performance of OO0 is significantly deteriorated when solving a cavity problem. For illustration purposes, the graphs of  $\left| \rho_{\lambda_{\text{open}}^{\text{OO0}}}^{\text{close}}(s) \right|$  and  $\left| \rho_{\lambda_{\text{open}}^{\text{OO0}}}^{\text{open}}(s) \right|$  are shown in Figure 3.

### 5.2.2 Evanescent modes damping operator (EMDA)

In the case of the EMDA symbol (29), the convergence radius  $\rho_{\lambda_{\text{open}}^{\text{EMDA}}}^{\text{close}}(s)$  writes

$$\rho_{\lambda_{\text{open}}^{\text{EMDA}}}^{\text{close}}(s) = \frac{-jk - (\lambda_{\text{close}}^{\text{opt}}(s) - \varepsilon k)}{-jk + (\lambda_{\text{close}}^{\text{opt}}(s) + \varepsilon k)},$$

and its modulus is given by:

$$\left| \rho_{\lambda_{\text{open}}^{\text{EMDA}}}^{\text{close}}(s) \right|^2 = \frac{k^2 + (\lambda_{\text{close}}^{\text{opt}}(s) - \varepsilon k)^2}{k^2 + (\lambda_{\text{close}}^{\text{opt}}(s) + \varepsilon k)^2}. \quad (34)$$

Depending on the values of  $\lambda_{\text{close}}^{\text{opt}}(s)$ , it is easy to see that  $\rho_{\lambda_{\text{open}}^{\text{EMDA}}}^{\text{close}}(s)$  exhibits the following properties:

1.  $\left| \rho_{\lambda_{\text{open}}^{\text{EMDA}}}^{\text{close}}(s) \right|^2 \rightarrow 1$  if  $\lambda_{\text{close}}^{\text{opt}}(s) \rightarrow \pm\infty$ ,  $\lambda_{\text{close}}^{\text{opt}}(s) \rightarrow 0$  or  $\varepsilon \rightarrow 0$ ;

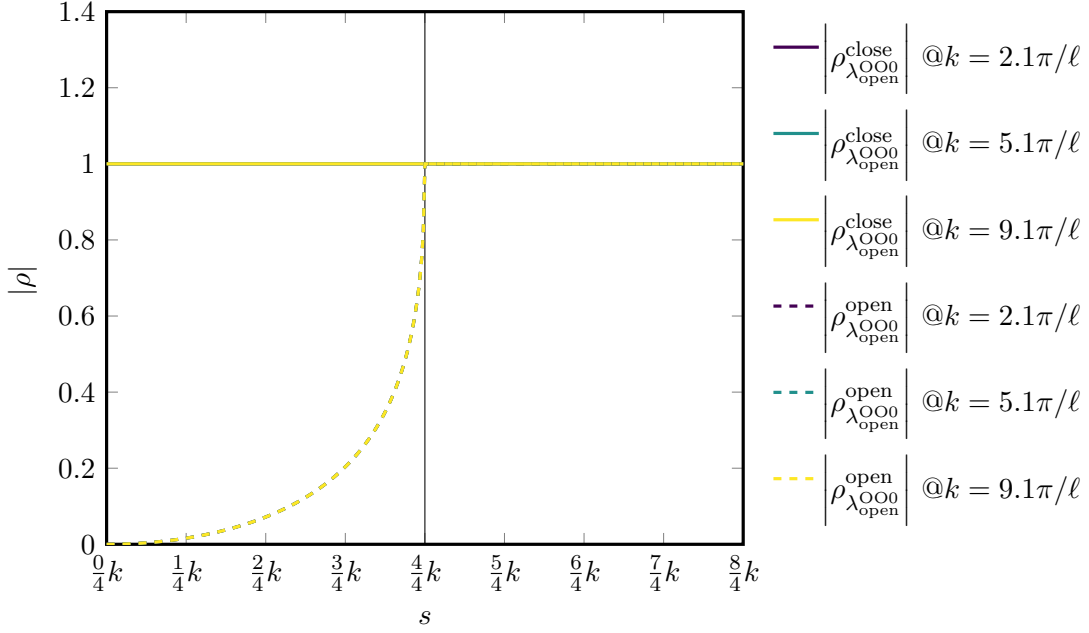


Figure 3: Graphs of  $\left|\rho_{\lambda_{\text{open}}}^{\text{close}}\right|$  and  $\left|\rho_{\lambda_{\text{open}}}^{\text{open}}\right|$  for different values of  $k$ .

2.  $\left|\rho_{\lambda_{\text{open}}}^{\text{close}}(s)\right|^2 < 1$  if  $\lambda_{\text{close}}^{\text{opt}}(s) > 0$  and  $\varepsilon > 0$ ;
3.  $\left|\rho_{\lambda_{\text{open}}}^{\text{close}}(s)\right|^2 > 1$  if  $\lambda_{\text{close}}^{\text{opt}}(s) < 0$  and  $\varepsilon > 0$ .

Obviously, the two last results are inverted for  $\varepsilon < 0$ .

Let us now compare  $\rho_{\lambda_{\text{open}}}^{\text{close}}$  and  $\rho_{\lambda_{\text{open}}}^{\text{open}}$  (*i.e.* the convergence radius of the EMDA operator when used in an OS scheme for solving the unbounded problem (21)). As shown in Figure 4 for a damping coefficient of  $\varepsilon = 25\%$ , the difference between the two radii becomes unnoticeable as  $s$  grows (once  $s^2 > k^2$ ). On the other hand, we have that:

$$\max_s \left| \rho_{\lambda_{\text{open}}}^{\text{open}}(s) \right| < 1 \quad (\text{see [9]}) \quad \max_s \left| \rho_{\lambda_{\text{open}}}^{\text{close}}(s) \right| > 1 \quad \forall s^2 < k^2.$$

In other words, the performance of EMDA is deteriorated when passing from an unbounded wave problem without obstacle to a cavity one.

### 5.2.3 Optimized second-order operator (OO2)

Let us now focus on the OO2 symbol (30). In this case, the convergence radius  $\rho_{\lambda_{\text{open}}}^{\text{close}}(s)$  is given by

$$\rho_{\lambda_{\text{open}}}^{\text{close}}(s) = \frac{(a + bs^2) - \lambda_{\text{close}}^{\text{opt}}(s)}{(a + bs^2) + \lambda_{\text{close}}^{\text{opt}}(s)},$$

and its modulus reads:

$$\left| \rho_{\lambda_{\text{open}}}^{\text{close}}(s) \right|^2 = \frac{|a + bs^2|^2 + [\lambda_{\text{close}}^{\text{opt}}(s)]^2 - 2\Re(a + bs^2)\lambda_{\text{close}}^{\text{opt}}(s)}{|a + bs^2|^2 + [\lambda_{\text{close}}^{\text{opt}}(s)]^2 + 2\Re(a + bs^2)\lambda_{\text{close}}^{\text{opt}}(s)}. \quad (35)$$

From this expression, it is clear that:

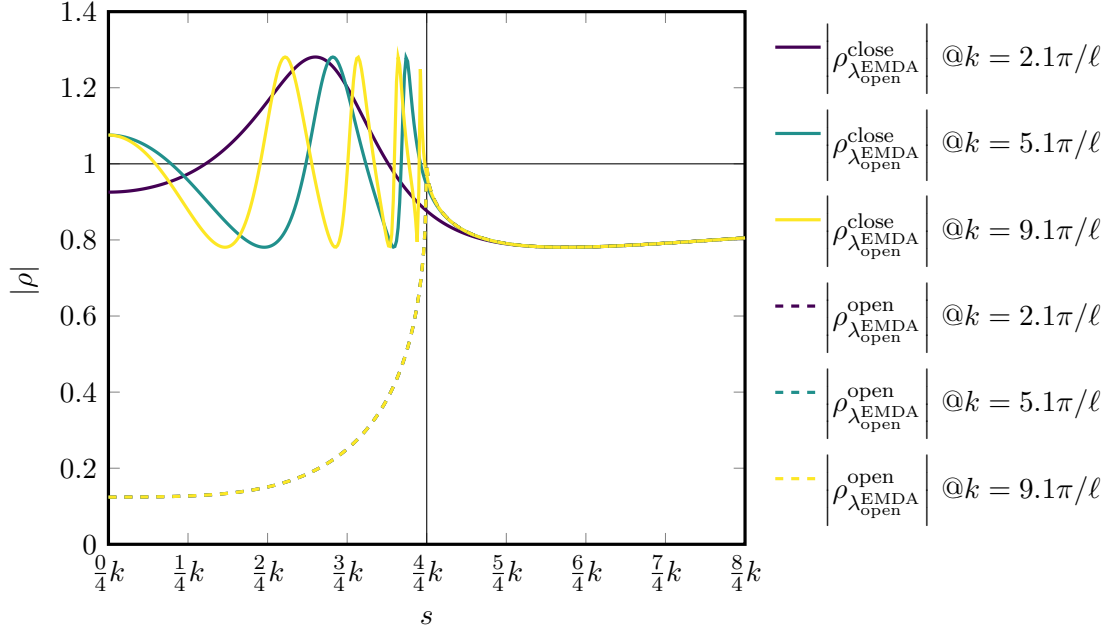


Figure 4: Graphs of  $\left| \rho_{\lambda_{\text{open}}^{\text{EMDA}}}^{\text{close}} \right|$  and  $\left| \rho_{\lambda_{\text{open}}^{\text{EMDA}}}^{\text{open}} \right|$  for different values of  $k$  and with  $\varepsilon = 0.25$ .

1.  $\left| \rho_{\lambda_{\text{open}}^{\text{close}}}^{\text{close}}(s) \right|^2 \rightarrow 1$  if  $\lambda_{\text{close}}^{\text{opt}}(s) \rightarrow \pm\infty$ ,  $\lambda_{\text{close}}^{\text{opt}}(s) \rightarrow 0$  or  $(a + bs^2) \rightarrow 0$ ;
2.  $\left| \rho_{\lambda_{\text{open}}^{\text{close}}}^{\text{close}}(s) \right|^2 < 1$  if  $\lambda_{\text{close}}^{\text{opt}}(s) > 0$  and  $\Re(a + bs^2) > 0$ ;
3.  $\left| \rho_{\lambda_{\text{open}}^{\text{close}}}^{\text{close}}(s) \right|^2 > 1$  if  $\lambda_{\text{close}}^{\text{opt}}(s) < 0$  and  $\Re(a + bs^2) > 0$ .

As with EMDA, the two last results are opposed for  $\Re(a + bs^2) < 0$ . Furthermore, it is worth noticing that, since  $\lambda_{\text{close}}^{\text{opt}}$  is changing its sign more than twice (at least for sufficiently large values of  $k$ ),  $a$  and  $b$  cannot be optimized to guarantee that  $\left| \rho_{\lambda_{\text{open}}^{\text{close}}}^{\text{close}}(s) \right|^2 < 1 \forall s^2 < k^2$ .

Figure 5 compares  $\left| \rho_{\lambda_{\text{open}}^{\text{close}}}^{\text{close}}(s) \right|$  with  $\left| \rho_{\lambda_{\text{open}}^{\text{open}}}^{\text{open}}(s) \right|$  (*i.e.* the convergence radius of the OO2 operator when used in an OS scheme for solving the unbounded problem (21)). Again, as expected, the distance between both radii becomes negligible as  $s$  grows (once  $s^2 > k^2$ ). Nonetheless, when analyzing non-evanescent modes, the performance of OO2 is poorer for cavity problems than for unbounded ones since:

$$\max_s \left| \rho_{\lambda_{\text{open}}^{\text{open}}}^{\text{open}}(s) \right| < 1 \text{ (see [10])} \quad \max_s \left| \rho_{\lambda_{\text{open}}^{\text{close}}}^{\text{close}}(s) \right| > 1 \quad \forall s^2 < k^2.$$

### 5.2.4 Square-root operator and its Padé localization (PADE)

In order to assess the performance of the PADE operator, let us first determine the performance of the square-root operator  $\mathcal{S}_{\text{open}}^{\text{opt}}$ , as given in (22), when used in the OS scheme (2) solving our model cavity problem (1). Indeed, as the Padé localization process leads to an excellent approximation of  $\mathcal{S}_{\text{open}}^{\text{opt}}$ , analyzing this limit case will shed light on the performance of the PADE operator, at least for a sufficiently large number of Padé terms  $N_p$ .

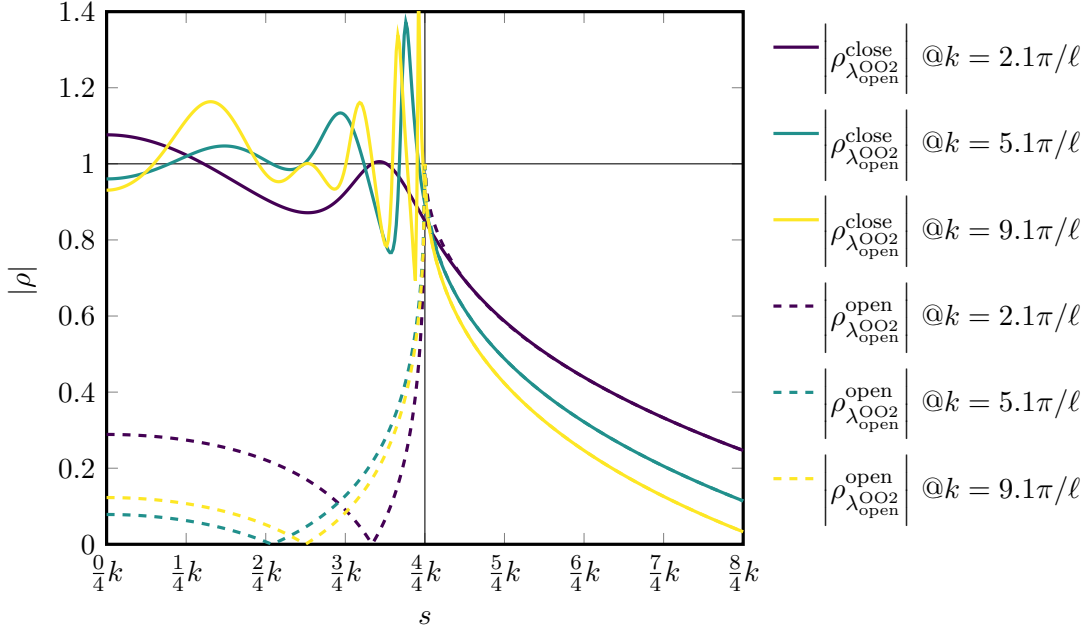


Figure 5: Graphs of  $\left|\rho_{\lambda_{\text{open}}^{\text{close}}}\right|$  and  $\left|\rho_{\lambda_{\text{open}}^{\text{open}}}\right|$  for different values of  $k$  (the values the coefficients  $a$  and  $b$ , as appearing in (30), are chosen according to [10]).

Given the expressions of  $\lambda_{\text{open}}^{\text{opt}}$  in (23), we can deduce that the convergence radius  $\rho_{\lambda_{\text{open}}^{\text{opt}}}^{\text{close}}$  writes

$$\rho_{\lambda_{\text{open}}^{\text{opt}}}^{\text{close}} = \begin{cases} \frac{-jk\sqrt{1 - \frac{s^2}{k^2}} - \sqrt{k^2 - s^2} \cot\left[\sqrt{k^2 - s^2} \frac{\ell}{2}\right]}{-jk\sqrt{1 - \frac{s^2}{k^2}} + \sqrt{k^2 - s^2} \cot\left[\sqrt{k^2 - s^2} \frac{\ell}{2}\right]} = \frac{-j - \cot\left[\sqrt{k^2 - s^2} \frac{\ell}{2}\right]}{-j + \cot\left[\sqrt{k^2 - s^2} \frac{\ell}{2}\right]} & \text{if } s^2 < k^2, \\ \frac{0 - 2/\ell}{0 + 2/\ell} = -1 & \text{if } s^2 = k^2, \\ \frac{k\sqrt{\frac{s^2}{k^2} - 1} - \sqrt{s^2 - k^2} \coth\left[\sqrt{s^2 - k^2} \frac{\ell}{2}\right]}{k\sqrt{\frac{s^2}{k^2} - 1} + \sqrt{s^2 - k^2} \coth\left[\sqrt{s^2 - k^2} \frac{\ell}{2}\right]} = \frac{1 - \coth\left[\sqrt{s^2 - k^2} \frac{\ell}{2}\right]}{1 + \coth\left[\sqrt{s^2 - k^2} \frac{\ell}{2}\right]} & \text{if } s^2 > k^2, \end{cases}$$

and therefore:

$$\left|\rho_{\lambda_{\text{open}}^{\text{opt}}}^{\text{close}}\right| = \begin{cases} 1 & \text{if } s^2 \leq k^2, & (36a) \\ \exp\left[-\ell\sqrt{s^2 - k^2}\right] & \text{if } s^2 > k^2, & (36b) \end{cases}$$

where the last line is obtained by directly exploiting the definition of the hyperbolic cotangent [20]. Before studying the convergence radius (36), it is worth mentioning that in the case  $s^2 < k^2$ ,  $\rho_{\lambda_{\text{open}}^{\text{opt}}}^{\text{close}}$  might be undefined because of the cotangent. However, the limit for  $s$  approaching a pole of the cotangent is well defined and is equal to  $-1$ . This can be easily shown by a direct application of L'Hôpital's rule. As expected, we have that  $\left|\rho_{\lambda_{\text{open}}^{\text{opt}}}^{\text{close}}\right|$  is identically equal to 1 for  $s^2 \leq k^2$  and decrease exponentially to 0 (once  $s^2 > k^2$ ) as  $s$  grows.

Let us now come back to the PADE operator. As its symbol (31) is obtained from a Padé approximation of  $\lambda_{\text{open}}^{\text{opt}}$ , and as this approximation converges to  $\lambda_{\text{open}}^{\text{opt}}$  as the number of Padé terms  $N_p \rightarrow \infty$  [21], we can argue that the convergence radius determined in (36) for the non-local square-

root operator approximates sharply the convergence radius  $\rho_{\lambda_{\text{open}}^{\text{PADE}}}^{\text{close}}$  of the PADE operator, at least for sufficiently large values of  $N_p$ , as show in Figure 6.

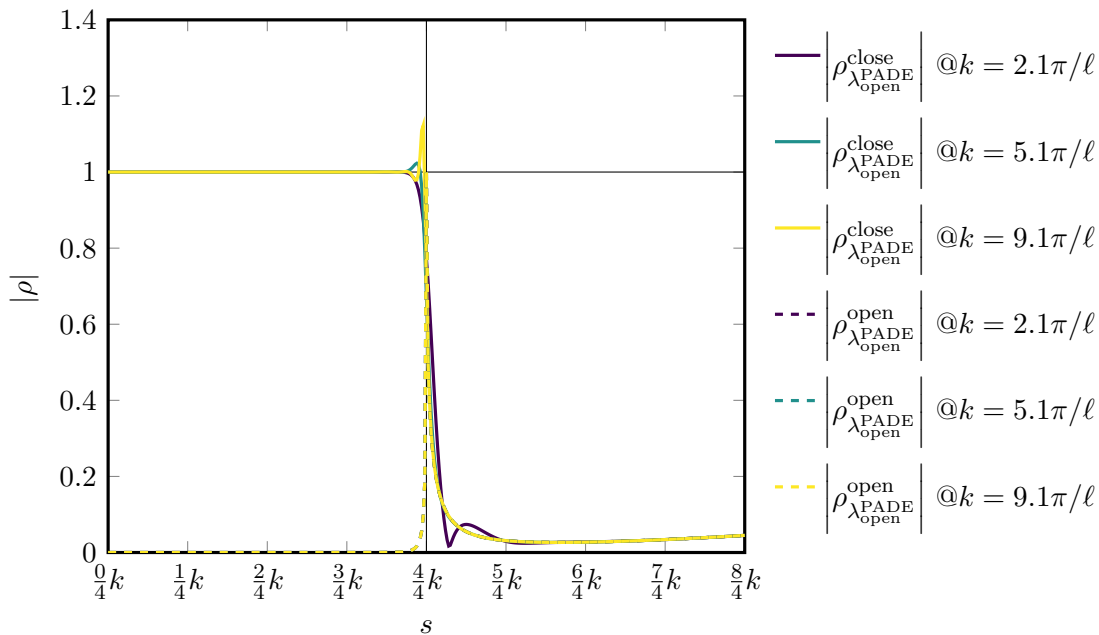


Figure 6: Graphs of  $\left| \rho_{\lambda_{\text{open}}^{\text{PADE}}}^{\text{close}} \right|$  and  $\left| \rho_{\lambda_{\text{open}}^{\text{PADE}}}^{\text{open}} \right|$  for different values of  $k$  an with  $N_p = 4$ .

### 5.2.5 Summary

Before concluding this section, let us summarize our analysis. When  $s^2 < k^2$ , we showed that  $\left| \rho_{\lambda_{\text{open}}^{\text{close, EMDA, OO2, PADE}}}^{\text{close}} \right|$  can be greater than 1. This behavior is significantly different from the unbounded case where  $\left| \rho_{\lambda_{\text{open}}^{\text{open, EMDA, OO2, PADE}}}^{\text{open}} \right|$  is always smaller than 1. On the other hand, when  $s^2 > k^2$ , the difference between  $\left| \rho_{\lambda_{\text{open}}^{\text{close, EMDA, OO2, PADE}}}^{\text{close}} \right|$  and  $\left| \rho_{\lambda_{\text{open}}^{\text{open, EMDA, OO2, PADE}}}^{\text{open}} \right|$  vanishes exponentially. Therefore, when comparing the OO2, EMDA, OO2 or PADE operators for solving *i*) a cavity problem similar to (1) with *ii*) an unbounded problem without obstacles similar to (21), we can conclude that the performance of the OS scheme will be deteriorated in the cavity case.

## 6 Numerical experiments and curved geometries

In this section, we carry out some numerical experiments in order to validate the previous theoretical analysis. Furthermore, as we restricted ourselves to rectangular geometries, we also offer in this section a numerical study of the performance of the aforementioned OS schemes when handling curved configurations: *i.e.* circles (2D) and spheres (3D).

### 6.1 Validation

Let us now illustrate the performance deterioration of the OO0, EMDA, OO2 and PADE transmission conditions, when used in an OS scheme for closed-domain Helmholtz problems. To this end, two different cases will be presented: *i*) a closed two-dimensional rectangular cavity with a length  $\ell = 9.5\lambda_w$ ,

where  $\lambda_w$  is the wavelength and *ii*) a section of an infinitely long two-dimensional rectangular waveguide with the same length  $\ell$ . In particular, the geometry displayed in Figure 7 is used and the following boundary conditions are imposed:

$$\begin{aligned}
p &= 0 && \text{on } \Gamma^{\infty/0} && \text{in the cavity case,} \\
\mathbf{n} \cdot \mathbf{grad} p &= jk && \text{on } \Gamma^{\infty/0} && \text{in the waveguide case,} \\
p &= 0 && \text{on } \Gamma^0 && \text{in both cases,} \\
p &= \sum_{m=1}^N \sin\left(m \frac{\pi}{h} y\right) && \text{on } \Gamma^s && \text{in both cases,}
\end{aligned} \tag{37}$$

where  $k = \frac{2\pi}{\lambda_w}$ ,  $h = \ell/2$  and  $N = 9$ . Let us stress that, as the length of the cavity is not an integer multiple of the wavelength, the closed Helmholtz problem is well defined. Furthermore, let us also note that 9 modes can propagate in the waveguide for the selected height and wavenumber. All these modes are superimposed when exciting both the cavity and the waveguide problems.

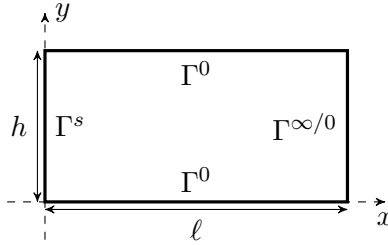


Figure 7: Rectangular geometry used for the numerical experiments.

Concerning the numerical setup, the Helmholtz problem (1) is discretized with a finite element method of order 5 and the geometry in Figure 7 is discretized with 8 triangular mesh elements per wavelength. An optimized Schwarz scheme is then used to solve (1a) with the boundary conditions given in (37), with  $g = 0$  and with two subdomains of equal size, as shown in Figure 1. Furthermore, let us mention that in the following numerical experiment, the non-overlapping fixed-point Schwarz algorithm is recast into the linear system [14]:

$$(\mathcal{I} - \mathcal{A})\mathbf{d} = \mathbf{b}, \tag{38}$$

where one application of the operator  $\mathcal{A}$  amounts to one iteration of the fixed-point procedure with *homogeneous* Dirichlet boundary conditions, where  $\mathcal{I}$  is the identity operator, where the vector  $\mathbf{d}$  concatenates all  $\mathbf{n} \cdot \mathbf{grad} p + \mathcal{S}(p)$  at the interface between the subdomains and where the right hand side vector  $\mathbf{b}$  results from the *non-homogeneous* Dirichlet boundary conditions. This linear system is then solved with a matrix-free GMRES *without* restart. Regarding the free parameters of the transmission conditions, we choose: 4 Padé terms and no damping for the PADE transmission condition [11]; the parameters  $\alpha, \beta$  for the OO2 operator as proposed in [10] and a damping of 25% for the EMDA operator as suggested in [22].

### 6.1.1 Convergence of GMRES

As a first numerical experiment, let us analyze the convergence rate of GMRES for solving both cavity and waveguide problems, as displayed in Figure 8. From these data, the performance loss in case of back-propagating waves (*i.e.* the cavity scenario) is obvious: a difference of 2 orders of magnitudes in the relative GMRES residual (between both scenarios) for OO2 and PADE.

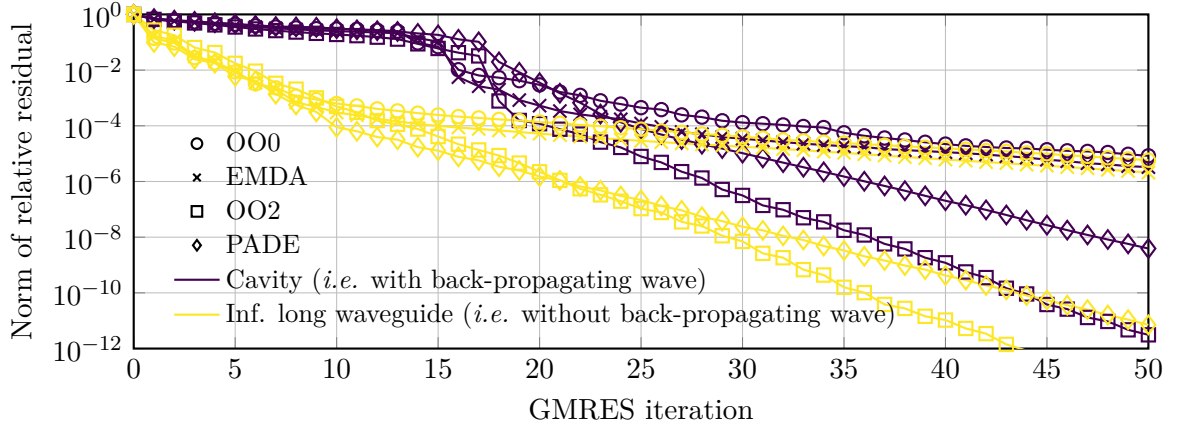


Figure 8: Convergence profile of GMRES for an infinitely long waveguide and for a cavity (two-dimensional rectangular case).

### 6.1.2 Spectrum of $\mathcal{I} - \mathcal{A}$

In a second numerical experiment, the spectrum of the system matrix  $\mathcal{I} - \mathcal{A}$  is studied for both rectangular cavity and waveguide cases. As shown in Figure 10, and as predicted by the theory, we can observe that for *cavity* problems:

1. all the eigenvalues lie *on* the unit circle for OO0;
2. some eigenvalues are located *outside* the unit circle for OO2 and EMDA and
3. all 9 non-evanescent modes lie *on* the unit circle for PADE.

For illustration purposes, a non-evanescent mode and an evanescent one are displayed in Figure 9. These modes are nothing else but eigenvectors of  $(\mathcal{I} - \mathcal{A})$ .

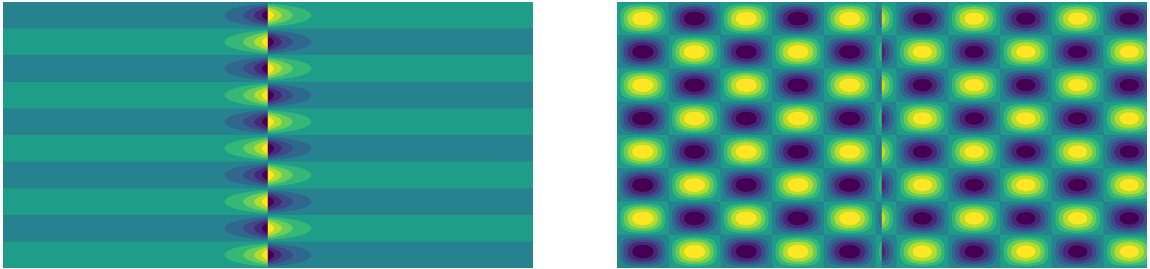


Figure 9: Evanescent (left) and non-evanescent (right) eigenmodes of  $(\mathcal{I} - \mathcal{A})$  (two-dimensional rectangular case).

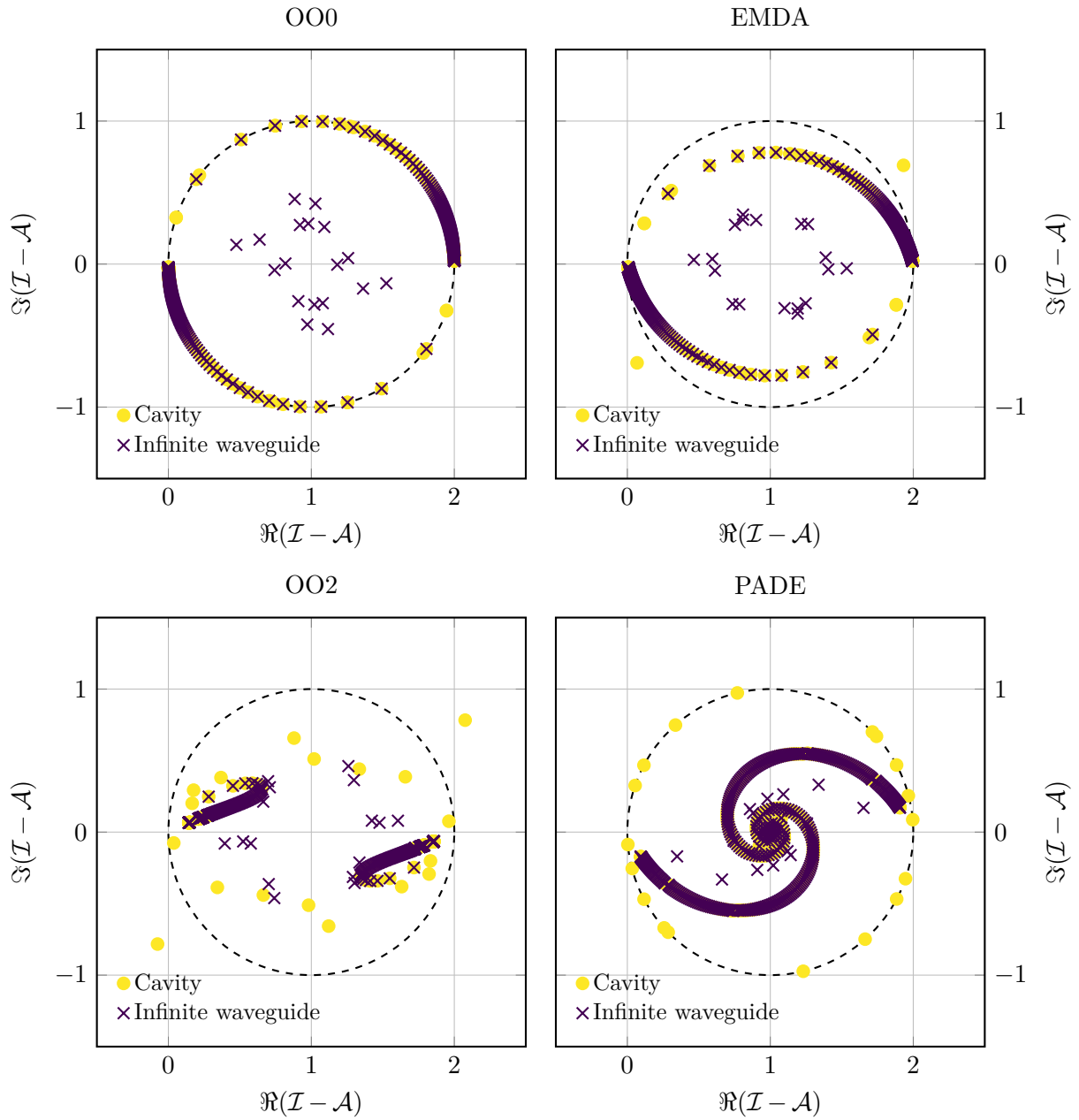


Figure 10: Spectrum of  $\mathcal{I} - \mathcal{A}$  with different transmission conditions (two-dimensional rectangular case).

## 6.2 Curved geometries

In the second part of this section, we study the behavior of the OO0, EMDA, OO2 and PADE transmission conditions when used in curved geometries (either open or closed) as shown in Figures 11 and 14 by numerical experiments. Let us note that in order to simplify the discussion, this subsection will consider *source-free* problems and thus focus on the spectrum of  $\mathcal{I} - \mathcal{A}$  only.

### 6.2.1 Two-dimensional case: a circular geometry

Let us start by considering a two-dimensional circular geometry with a radius  $R_c$  such that  $2R_c = 9.5\lambda_w$ . In contrast to the previous test case, a circular (concentric) domain decomposition is chosen, and in order to consider a configuration with more than two subdomains we adopt here a *four* subdomains setting. Regarding the discretization, we use again the boundary conditions (37)<sup>5</sup> and discretize the Helmholtz problem with a finite element method of order 5 on a geometry meshed with 8 *curved* (second-order) triangular elements per wavelength. Concerning the free parameters of the transmission operators, we choose: 4 Padé terms without damping for the PADE condition; the parameters  $\alpha, \beta$  of the OO2 condition as proposed in [11] and a damping of 50% for the EMDA condition as suggested in [9]. For illustration purposes, a schematic representation of the numerical setting is shown in Figure 11.

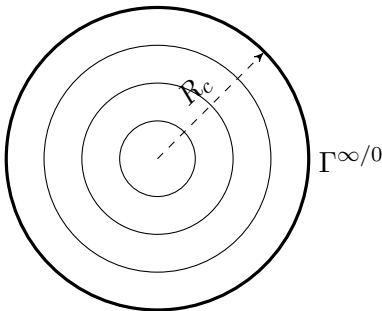


Figure 11: Two-dimensional circular geometry used for the numerical experiments.

The spectra of  $\mathcal{I} - \mathcal{A}$  for open and closed problems and for the different transmission conditions are depicted in Figure 12. As it can be directly seen from those data, the conclusions drawn in section 5.2 are once again recovered. Indeed, in the case of a cavity problem: *i*) all eigenvalues lie on the unit circle with the OO0 condition; *ii*) some eigenvalues are outside the unit circle with the EMDA and OO2 operators and *iii*) some eigenvalues lie on the unit circle with the PADE condition. Let us also note that the number of eigenvalues lying on the unit circle for the PADE operator in the closed case should match the number of eigenvalues *inside* the unit circle for the OO0 condition in the *open* case. This behavior is recovered, up to a few modes near the unit circle (*i.e.*  $|\text{Eig } \mathcal{A}| \simeq 0.9$ ), as shown in Figure 13.

<sup>5</sup>Let us note that the boundary conditions on  $\Gamma^0$  and  $\Gamma^s$  are simply ignored in this case. Furthermore, the condition  $\mathbf{n} \cdot \mathbf{grad } p = jk$  in (37) is no longer an *exact* absorbing boundary condition in this curved setting.

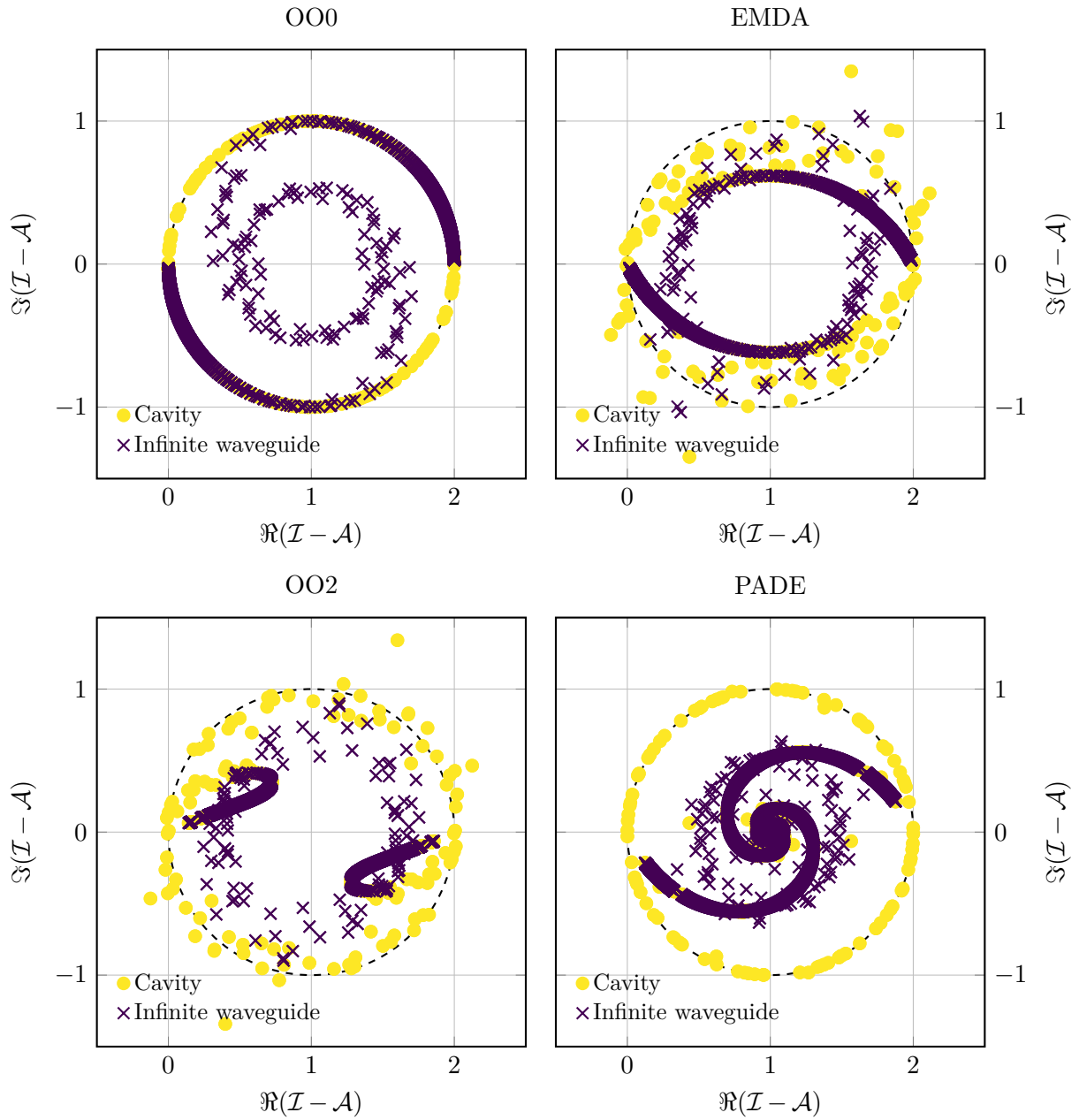


Figure 12: Spectrum of  $\mathcal{I} - \mathcal{A}$  with different transmission conditions (two-dimensional circular case with four subdomains).

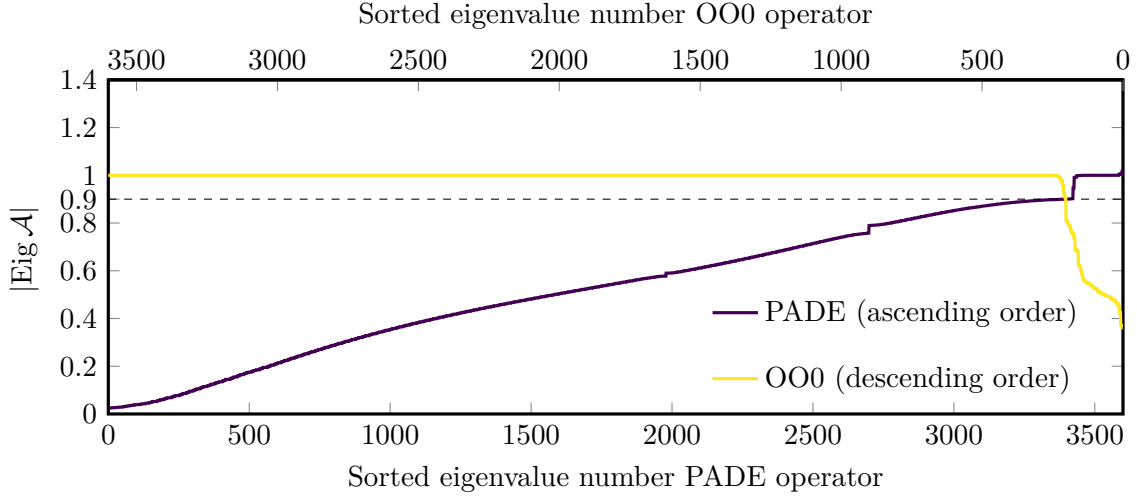


Figure 13: Modulus of the eigenvalues of  $\mathcal{A}$  with PADE (closed problem) and OO0 (open problem); the eigenvalues are sorted in: *i*) ascending order with PADE and *ii*) descending order with OO0 (two-dimensional circular case with four subdomains).

### 6.2.2 Three-dimensional case: a spherical geometry

For this last numerical experiment, a three-dimensional case is studied. In particular, we extend the previous two-dimensional circular scenario to a three-dimensional spherical problem, as shown in Figure 14. However, in order to keep the computational effort reasonable, this last numerical experiment is restricted to: *i*) a sphere radius  $R_s$  such that  $2R_s = 3.5\lambda_w$ ; *ii*) two subdomains and *iii*) a second-order finite element discretization. All other numerical aspects, such as the free parameters of the transmission operators, are kept identical to the previous study.

Once again, we compute the spectra of  $\mathcal{I} - \mathcal{A}$  for open and closed problems and for the different transmission conditions. From the data depicted in Figure 15, it is obvious that the conclusions we have drawn in the previous two-dimensional numerical experiments remain once again valid. In particular: *i*) all eigenvalues lie on the unit circle with the OO0 condition; *ii*) some eigenvalues are outside the unit circle with the EMDA and OO2 operators and *iii*) some eigenvalues lie on the unit circle with the PADE condition. Regarding this last point, we recover that the number of eigenvalues lying on the unit circle for the PADE operator in the closed case matches (up to a few eigenvalues near  $|\text{Eig } \mathcal{A}| \simeq 0.9$ ) the number of eigenvalues *inside* the unit circle for the OO0 condition in the *open* case, as shown in Figure 16.

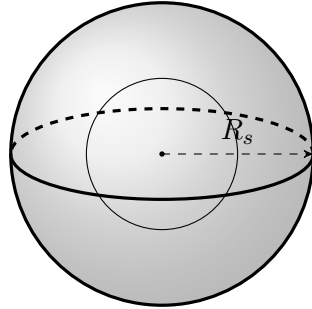


Figure 14: Three-dimensional spherical geometry used for the numerical experiments.

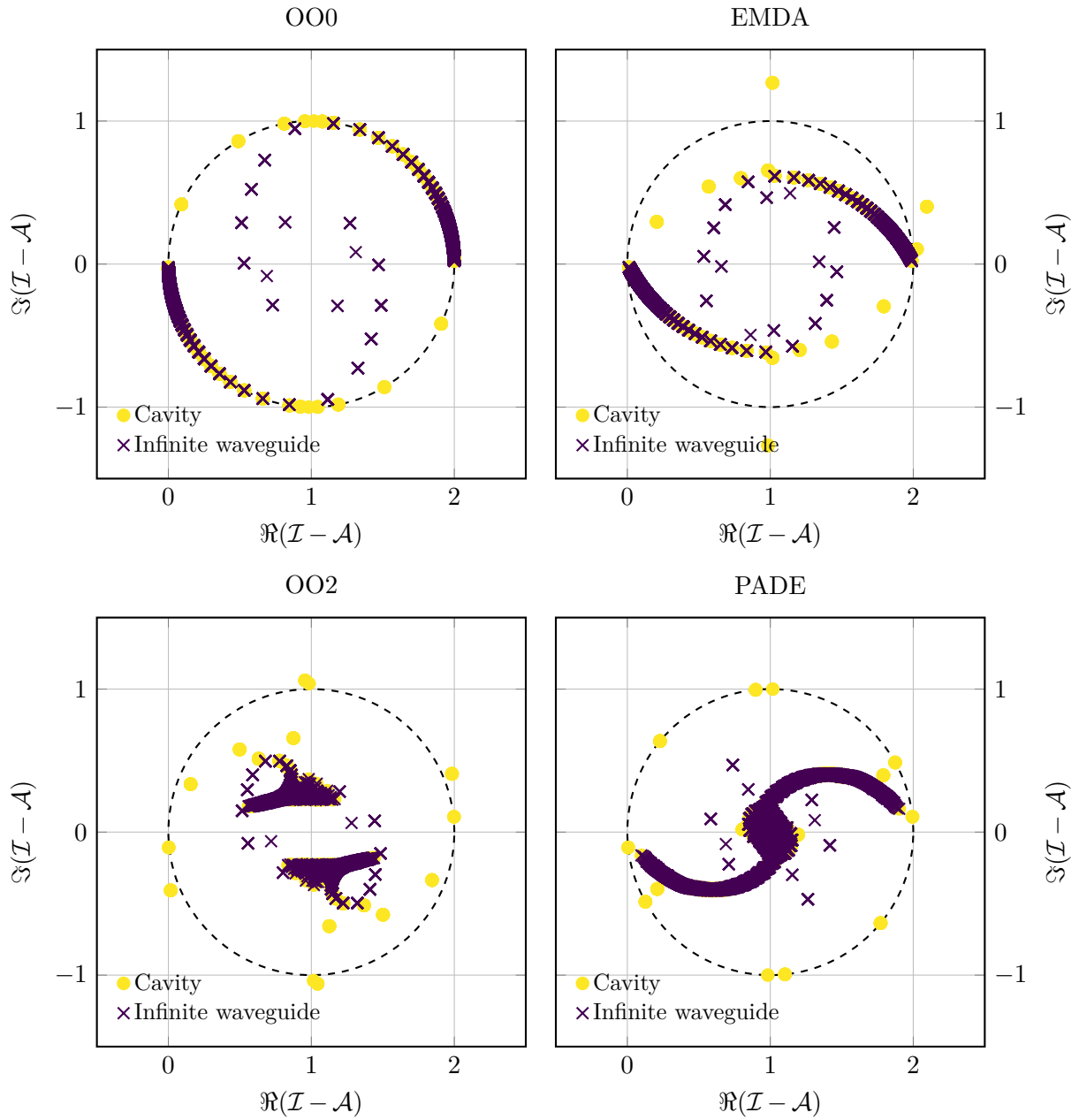


Figure 15: Spectrum of  $\mathcal{I} - \mathcal{A}$  with different transmission conditions (three-dimensional spherical case).

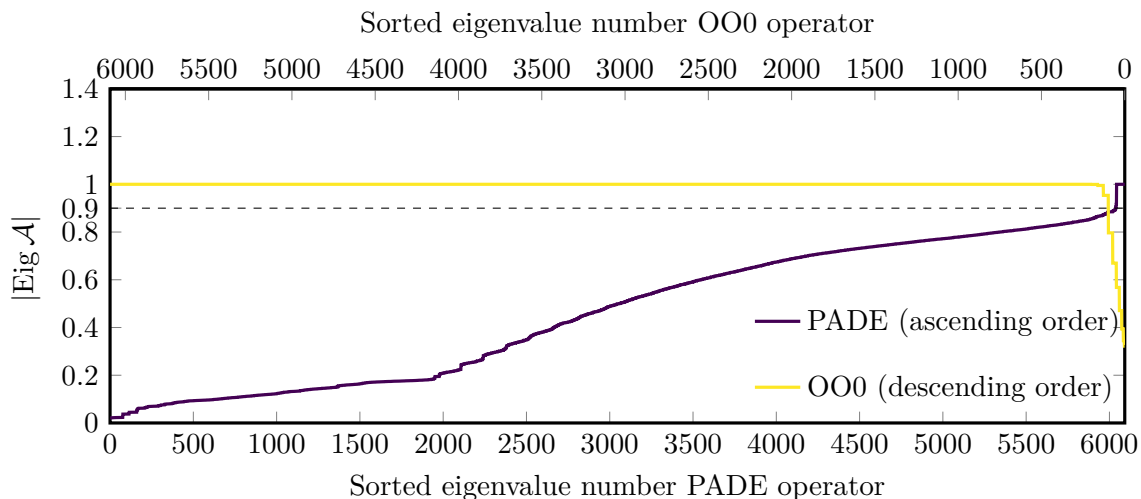


Figure 16: Modulus of the eigenvalues of  $\mathcal{A}$  with PADE (closed problem) and OO0 (open problem); the eigenvalues are sorted in: *i*) ascending order with PADE and *ii*) descending order with OO0 (three-dimensional spherical case with two subdomains).

## 7 Conclusion

In this paper, we derived the optimal transmission operator  $\mathcal{S}_{\text{close}}^{\text{opt}}$  of an optimized Schwarz scheme solving a simple rectangular Helmholtz cavity problem. We furthermore demonstrated that for *evanescent* modes this optimal operator is excellently approximated by the optimal transmission operator of open problems without obstacles  $\mathcal{S}_{\text{open}}^{\text{opt}}$ . On the other hand, we also showed that  $\mathcal{S}_{\text{open}}^{\text{opt}}$  cannot be used to approximate  $\mathcal{S}_{\text{close}}^{\text{opt}}$  for *non-evanescent* modes. For this reason the classical OO0, EMDA, OO2 and PADE transmission operators exhibit a performance drop when applied to cavity problems (compared to an equivalent unbounded configuration). In particular, we determined that the convergence radius  $\rho^{\text{close}}(s)$  of the OS scheme exhibits:

1. a modulus equal to 1 for all  $s \in \mathbb{R}$  for the OO0 operator;
2. a modulus greater than 1 for some  $s^2 < k^2$  for the EMDA and OO2 operators and
3. a modulus equal to 1 for all  $s^2 \leq k^2$  for the PADE operator, at least when using a sufficiently large number of Padé terms.

Furthermore, by means of numerical experiments, we showed that those conclusions, which were derived for a rectangular domain, remain valid when considering curved and three-dimensional configurations.

## Acknowledgments

This research project has been funded by the Deutsche Forschungsgemeinschaft (DFG, German Research Foundation) – Project number 445906998. The authors would like to express their gratitude to Ms. Heike Koch, Mr. Achim Wagner, Mr. Dragos Munteanu and Dr. Wolfgang Müller for the administrative and technical support.

## References

- [1] F. Ihlenburg and I. Babuška, “Finite element solution of the Helmholtz equation with high wave number part I: The h-version of the FEM,” *Computers & Mathematics with Applications*, vol. 30, no. 9, pp. 9–37, 1995.
- [2] O. G. Ernst and M. J. Gander, “Why it is difficult to solve Helmholtz problems with classical iterative methods,” in *Numerical Analysis of Multiscale Problems* (I. G. Graham, T. Y. Hou, O. Lakkis, and R. Scheichl, eds.), vol. 83 of *Lecture Notes in Computational Science and Engineering*, pp. 325–363, 2012.
- [3] F. Ihlenburg and I. Babuška, “Finite element solution of the Helmholtz equation with high wave number part II: The h-p version of the FEM,” *SIAM Journal on Numerical Analysis*, vol. 34, no. 1, pp. 315–358, 1997.
- [4] A. Moiola and E. A. Spence, “Is the Helmholtz equation really sign-indefinite?,” *SIAM Review*, vol. 56, no. 2, pp. 274–312, 2014.
- [5] G. C. Diwan, A. Moiola, and E. A. Spence, “Can coercive formulations lead to fast and accurate solution of the Helmholtz equation?,” *Journal of Computational and Applied Mathematics*, vol. 352, pp. 110–131, 2019.
- [6] M. Yannakakis, “Computing the minimum fill-in is NP-complete,” *SIAM Journal on Algebraic Discrete Methods*, vol. 2, no. 1, pp. 77–79, 1981.
- [7] N. Marsic, H. De Gerssem, G. Demésy, A. Nicolet, and C. Geuzaine, “Modal analysis of the ultrahigh finesse Haroche QED cavity,” *New Journal of Physics*, vol. 20, no. 4, p. 043058, 2018.
- [8] B. Després, “Décomposition de domaine et problème de Helmholtz,” *Comptes Rendus de l’Académie des Sciences*, vol. 311, pp. 313–316, 1990.
- [9] Y. Boubendir, “An analysis of the BEM-FEM non-overlapping domain decomposition method for a scattering problem,” *Journal of Computational and Applied Mathematics*, vol. 204, no. 2, pp. 282–291, 2007.
- [10] M. J. Gander, F. Magoulès, and F. Nataf, “Optimized Schwarz methods without overlap for the Helmholtz equation,” *SIAM Journal on Scientific Computing*, vol. 24, no. 1, pp. 38–60, 2002.
- [11] Y. Boubendir, X. Antoine, and C. Geuzaine, “A quasi-optimal non-overlapping domain decomposition algorithm for the Helmholtz equation,” *Journal of Computational Physics*, vol. 231, no. 2, pp. 262–280, 2012.
- [12] A. Vion and C. Geuzaine, “Double sweep preconditioner for optimized Schwarz methods applied to the Helmholtz problem,” *Journal of Computational Physics*, vol. 266, pp. 171–190, 2014.
- [13] M. J. Gander and H. Zhang, “A class of iterative solvers for the Helmholtz equation: Factorizations, sweeping preconditioners, source transfer, single layer potentials, polarized traces, and optimized Schwarz methods,” *SIAM Review*, vol. 61, no. 1, pp. 3–76, 2019.
- [14] V. Dolean, P. Jolivet, and F. Nataf, *An introduction to domain decomposition methods: algorithms, theory and parallel implementation*. Society for Industrial and Applied Mathematics, 2015.

- [15] Z. Peng and J.-F. Lee, “Non-conformal domain decomposition method with mixed true second order transmission condition for solving large finite antenna arrays,” *IEEE Transactions on Antennas and Propagation*, vol. 59, no. 5, pp. 1638–1651, 2011.
- [16] P.-H. Tournier, M. Bonazzoli, V. Dolean, F. Rapetti, F. Hecht, F. Nataf, I. Aliferis, I. El Kanfoud, C. Migliaccio, M. de Buhan, M. Darbas, S. Semenov, and C. Pichot, “Numerical modeling and high-speed parallel computing: New perspectives on tomographic microwave imaging for brain stroke detection and monitoring,” *IEEE Antennas and Propagation Magazine*, vol. 59, no. 5, pp. 98–110, 2017.
- [17] N. Marsic, C. Waltz, J.-F. Lee, and C. Geuzaine, “Domain decomposition methods for time-harmonic electromagnetic waves with high order whitney forms,” *IEEE Transactions on Magnetics*, vol. 52, no. 3, pp. 1–4, 2016.
- [18] B. E. A. Saleh and M. C. Teich, *Fundamentals of Photonics*. Wiley-Interscience, 2 ed., 2007.
- [19] K. Ko, N. Folwell, L. Ge, A. Guetz, L. Lee, Z. Li, C. Ng, E. Prudencio, G. Schussman, R. Uplenchwar, and L. Xiao, “Advances in electromagnetic modelling through high performance computing,” *Physica C: Superconductivity and its Applications*, vol. 441, no. 1-2, pp. 258–262, 2006.
- [20] K. Oldham, J. Myland, and J. Spanier, *An Atlas of Functions*. Springer-Verlag New York, 2 ed., 2009.
- [21] X. Antoine, M. Darbas, and Y. Y. Lu, “An improved surface radiation condition for high-frequency acoustic scattering problems,” *Computer Methods in Applied Mechanics and Engineering*, vol. 195, no. 33-36, pp. 4060–4074, 2006.
- [22] N. Marsic, *Efficient methods for large-scale time-harmonic wave simulations*. PhD thesis, Université de Liège, Belgique, 2016.